



Anna Franziska Purkhauser, BSc

**On the Use of Doppler Measurements
for Dynamic Orbit Computation.
Case Study: GRAIL**

MASTER'S THESIS

to achieve the university degree of

Diplom-Ingenieurin

Master's degree programme: Geomatics Science

submitted to

Graz University of Technology

Supervisor

Dr. Oliver Baur

Institute of Geodesy

AFFIDAVIT

I declare that I have authored this thesis independently, that I have not used other than the declared sources/resources, and that I have explicitly indicated all material which has been quoted either literally or by content from the sources used. The text document uploaded to TUGRAZonline is identical to the present master's thesis dissertation.

Date

Signature

Abstract

The trajectory computation of lunar/planetary orbiters is based on Radio Science ([RS](#)) data. [RS](#) data include signal travel time and frequency shift (Doppler) measurements between ground stations and the spacecraft. This raw data can be converted to range and range-rate observations, respectively. The latter are eventually used as observations in dynamic orbit computation. Within the dynamic orbit determination process, all (gravitational and non-gravitational) forces acting on a satellite are modelled and/or parametrized in such a way, that the difference between the observed and computed ranges/range-rates becomes minimal in a least-squares sense.

In the following case study, the interplanetary mission Gravity Recovery and Interior Laboratory ([GRAIL](#)) was chosen. Its twin-satellites were orbiting the Moon and tracked by the Deep Space Network ([DSN](#)).

The motivation of this master thesis is the computation of the orbit of the [GRAIL](#) spacecraft from [RS](#) data (Doppler measurements only) provided by the National Aeronautics and Space Administration ([NASA](#)) via the Planetary Data System ([PDS](#)). The main focus is the treatment of Doppler measurements. The tasks are as follows:

- Conversion of the raw Doppler measurements to range-rate observations
 - File formats and contents
 - Data types
 - Computation of range-rates
 - Correction for atmospheric and relativistic effects
- Orbit computation from range-rate observations with the Goddard Space Flight Center ([GSFC](#)) [GEODYN II](#) software package
- Comparison of obtained orbits with those published by [NASA](#) (e.g. [SPICE](#) kernels)

Zusammenfassung

Die Trajektorien- bzw. Bahnbestimmung von interplanetaren Satelliten basiert auf Radio Science (RS) Daten. Diese Daten umfassen die Signallaufzeit und Frequenzverschiebung bzw. Dopplermessungen zwischen Bodenstationen und Satelliten. In weiterer Folge können die Rohdaten zu Distanzen sowie Distanzänderungen umgewandelt und als Beobachtungen in der dynamischen Orbitberechnung verwendet werden. Bei der dynamischen Bahnbestimmung werden alle (sowohl gravitative als auch nicht-gravitative) Kräfte, die auf den Satelliten wirken, modelliert bzw. parametrisiert, sodass die Differenz zwischen gemessenen und berechneten Beobachtungen minimal - im Sinne der Ausgleichungsmethode der kleinsten Quadrate - werden.

In der vorliegenden Fallstudie wird als Studienobjekt die Mondmission Gravity Recovery and Interior Laboratory (GRAIL) verwendet. Ihre Zwillingssatelliten umkreisten hintereinander im gleichen Orbit den Mond und wurden vom Deep Space Network (DSN) getrackt.

Die Motivation der vorliegenden Thesis ist die Orbitbestimmung der GRAIL Satelliten mittels RS Daten (nur Dopplermessungen), die von der National Aeronautics and Space Administration (NASA) via Planetary Data System (PDS) zur Verfügung stehen. Der Fokus liegt dabei in der Behandlung der Doppler Messungen. Die Aufgaben sind wie folgt:

- Konvertierung der Doppler Rohdaten zu Distanzänderungen
 - Datenformate und ihre Inhalte
 - Datentypen
 - Berechnung der Distanzänderungen
 - Korrekturen für atmosphärische und relativistische Effekte
- Orbitbestimmung mittels Distanzänderungen mit dem Goddard Space Flight Center (GSFC) GEODYN II Softwarepaket
- Vergleich des berechneten Orbits mit publizierten Ergebnissen der NASA (z.B. SPICE Kernel)

Das, wobei unsere Berechnungen versagen, nennen wir Zufall.
Albert Einstein

Contents

List of Figures	VIII
List of Tables	IX
Listings	X
Acronyms and Abbreviations	XI
1. Introduction	1
2. Theoretical Background	3
2.1. Radio Science	3
2.1.1. Doppler Shift	3
2.1.2. Observation Principle	5
2.1.3. Tracking	7
2.2. Orbit Determination	7
2.2.1. Forces Acting on a Satellite	9
2.3. Time and Reference Systems	9
2.3.1. Time Scales	10
2.3.2. Time Differences	11
2.3.3. Reference Systems	11
3. GRAIL Mission	14
3.1. Orbit	15
3.2. Spacecraft	15
3.3. Ranging System	16
3.4. Tracking Network	17
4. Data	19
4.1. Observable	19
4.2. Data Formats	20
4.2.1. ODF Tracking Data Format	20
4.2.2. WEA File Format	26

Contents

5. Methodology	28
5.1. Light Time Solution	30
5.1.1. Round Trip Light Time	30
5.1.2. Light Time Equation	31
5.1.3. Algorithm	32
5.2. Range Difference	34
5.2.1. Algorithm	36
5.3. Observation Corrections	38
5.3.1. Tropospheric Correction	38
5.3.2. Relativistic Correction	40
5.4. Ramped Frequency	40
5.5. Overview	41
6. Results	44
6.1. Files Formats and Contents	44
6.2. Orbit Determination	49
6.3. Range-Rate Determination	53
6.4. Numerical Considerations	53
7. Conclusion	57
Bibliography	XIII
A. G2B Tracking Data Format	XVII
B. Tracking Data Format Conversion	XXII
B.1. LIGHTT File	XXV
B.2. SATID File	XXV
C. GEODYN II	XXVII
C.1. Input	XXVII
C.2. Modelling	XXVIII
C.3. Processing	XXIX

List of Figures

2.1.	Example of a Doppler shift for a received signal	4
2.2.	1-, 2- and 3-way Doppler measurements	5
2.3.	Doppler extraction process	6
2.4.	Orbit determination approaches	7
3.1.	GRAIL mission	14
3.2.	Top view of the GRAIL spacecraft	15
3.3.	Global distribution of DSN	17
5.1.	Schematic overview of the radio navigation process	29
5.2.	Notation for light time solution	30
5.3.	Schema for 1-way Doppler range-rate determination	36
5.4.	Observation computation	43
6.1.	1- and 2-way Doppler data	46
6.2.	Reference frequencies in the 2-way Doppler data	46
6.3.	Ramped frequency	47
6.4.	Observation difference	48
6.5.	Time difference	48
6.6.	Orbit comparison to JPL	50
6.7.	Orbit comparison to JPL	50
6.8.	Orbit comparison to JPL	51
6.9.	1st and last iteration residuals	52
6.10.	Last iteration residuals with marked outliers	52
6.11.	Computed observable compared to GEODYN solution	54
6.12.	Difference of computed observable with GEODYN solution	54
6.13.	Computed observable compared to GEODYN solution	55
6.14.	Difference of computed observable with GEODYN solution	55
B.1.	Conversion process	XXVI
C.1.	Observation generation in GEODYN II	XXXI

List of Tables

3.1. Uplink and downlink frequencies for DSN	16
3.2. Turn-around ratios	16
3.3. Primary DSN tracking stations supporting GRAIL	17
3.4. Coordinates of the primary DSN tracking stations	18
3.5. Site velocities for DSS	18
4.1. ODF layout	21
4.2. ODF orbit data group	24
4.3. ODF ramp data group	25
4.4. WEA header format	25
4.5. WEA data format	25
6.1. Pre-launch and observed tracking noise	45
A.1. G2B layout	XVII
A.2. G2B msster block header record	XVIII
A.3. G2B block header record	XIX
A.4. G2B ramp header record	XIX
A.5. G2B observation record	XX
A.6. G2B observation correction record	XX
A.7. G2B ramp record	XX
A.8. G2B weather data	XXI

Listings

4.1. ODF file	23
4.2. WEA file	27
B.1. ODF file	XXIV
B.2. G2B file	XXIV
B.3. LIGHTT file	XXV

Acronyms and Abbreviations

ASCII	American Standard Code for Information Interchange
BCRS	Barycentric Celestial Reference System
DOY	Day of Year
DSCC	Deep Space Communications Complexes
DSN	Deep Space Network
DSS	Deep Space Station
EDR	Experimental Data Record
ET	Ephemeris Time
G2B	GEODYN II Binary
GCRS	Geocentric Celestial Reference System
GEODYN	GSFC processing code for orbit determination
GNSS	Global Navigation Satellite System
GRAIL	Gravity Recovery and Interior Laboratory
GSFC	Goddard Space Flight Center
ICRF	International Celestial Reference Frame
ICRS	International Celestial Reference System
IERS	International Earth Rotation and Reference Systems Service
ITRF	International Terrestrial Reference Frame
ITRS	International Terrestrial Reference System
JD	Julian Date
JPL	Jet Propulsion Laboratory
LGRS	Lunar Gravity and Ranging System

Listings

MATLAB	Matrix Laboratory
MJD	Modified Julian Date
MJDS	Modified Julian Date Seconds
NASA	National Aeronautics and Space Administration
OD	Orbit Determination
ODF	Orbit Data File
PDS	Planetary Data System
RS	Radio Science
SI	International System of Units
SPICE	Spacecraft Planet Instrument "C-Matrix" Event
TAI	International Atomic Time
TDB	Barycentric Dynamic Time
TDF	Tracking Data Format
TDT	Terrestrial Dynamic Time
USA	United States of America
UT	Universal Time
UTC	Coordinated Universal Time
VLBI	Very Long Baseline Interferometry
WEA	Weather

Chapter 1.

Introduction

Since the beginning of human history, humankind has been studying outer space and, more specifically, our solar system. The first observations were based on measurement systems that relied on visible light. That is why it was only possible to perform long-range and indirect measurements. With the discovery of radio waves a new area began. Since that time, radio signal observations were used to investigate celestial objects.

With the beginning of the space flight era, new measurement platforms emerged. Since then instruments can operate above the Earth's atmosphere on a spacecraft or satellite. Therefore, the whole electromagnetic spectrum can be used and the observations are not affected by the Earth's atmosphere. The latest developments in the area of interplanetary travel makes it possible to carry instruments to various planetary and celestial bodies in the solar system. Hence, the physical properties and dynamics can be measured directly and at very close range (Doody, 2001).

With all these possibilities, our knowledge about the solar system is growing rapidly. Nevertheless, there are still many unanswered questions about the evolutionary history of the terrestrial planets. The most accessible planetary body to answer this queries is the Moon. Its surface preserved the history of most of the solar systems past. But to reconstruct the evolution, a deep understanding of the interior is necessary. The structure of a planet's interior contains information regarding the bulk composition, differentiation and the nature of heat generation and heat loss, which influence the style, extant and duration of volcanism and tectonics (Zuber et al., 2013a).

The **GRAIL** mission was undertaken to seek answers to these fundamental questions on lunar evolution. Its task was to map the lunar gravitational field, since gravity is the primary means of mapping the mass distribution of the interior. A spacecraft in orbit is perturbed by the distribution of mass, particularly of its central body. To fulfil the given assignment, the two spacecraft's of the **GRAIL** mission were orbiting the Moon in a low altitude of 50 km (Zuber et al., 2013b).

The most common technique to track a satellite, especially in the interplanetary case, is the **RS** Doppler measurement principle. The method is based on the detection of a

Chapter 1. Introduction

change in frequency of the radio signal, known as Doppler shift. The observed data can be converted to range-rate observables. This computed observable is necessary for the determination of the orbit and subsequently, the gravity field.

The aim of this master thesis is to follow the processing of the Doppler shift data from the observation by the DSN till the determination of the computed observable in the case of GRAIL. The computed observable is part of the orbit determination problem. A widely used software package for orbit and gravity field determination is the GSFC processing code for orbit determination (GEODYN) II software. The question arises, how exactly the observation is treated and the computed observable is calculated. So the task is to firstly understand the process behind GEODYN. As a second step the procedure of the observation determination till the computation of the residuals is implemented accordingly in Matrix Laboratory (MATLAB), while GEODYN is used as a reference.

To give a background to the observation processing the basics of the RS technique and its observation principle are presented in chapter 2. Also the general procedure of the orbit determination is described. Additionally, the used time and reference systems are defined in section 2.3.

Chapter 3 gives an overview of the satellite mission GRAIL. In addition, the details of the spacecraft, its orbit and the tracking network DSN are described. The measured data is detailed in chapter 4. The focus lies on the observation itself and on the DSN tracking data format, namely the Orbit Data File (ODF).

In chapter 5 the process from the raw measurement to the computed observable, namely the range-rate, is addressed. The light time solution and range-rate determination as well as the ramped frequency and their sequence in the observation computation process is described.

Chapter 6 finally summarizes the found results in a sequential form, starting with the file formats and their content. Afterwards a short section details the modelling in GEODYN and compares the computed orbit with the official Jet Propulsion Laboratory (JPL) orbit solution. The chapter concludes with the results of the self written range-rate determination in comparison with the GEODYN result as reference. Finally, chapter 7 summarizes and discusses the results of this thesis. Also a possible future research focus is outlined.

The appendix focuses on the GEODYN software package and its tracking data file format GEODYN II Binary (G2B). Firstly the G2B format is described. Then the conversion process of the ODF to the G2B format is detailed. In this context additional files for the conversion routine are defined. The last chapter focusses on GEODYN, its input, modelling and observation processing.

Chapter 2.

Theoretical Background

2.1. Radio Science

RS techniques observe the signal travel time and frequency of a spacecraft's carrier link between the orbiter and the Earth tracking station. The observed frequency can be seen in relation to the transmitted frequency. The difference, the so called frequency shift or Doppler effect, of the radio signal is proportional to the relative velocity change between spacecraft and ground station. In addition, the measured radio signals are affected by

- the gravitational influence of planetary bodies (i.e. relativistic effects),
- the media through which they propagate (e.g. atmosphere, troposphere) and
- the performance of the various systems on the spacecraft and on Earth needed in the process (e.g. station delays, wavelength).

The **RS** measurement principle is therefore based on the detection of a change in the frequency of the radio signal and enables for example the determination of an orbit and estimation of gravitational parameters ([Andert, 2010](#)).

2.1.1. Doppler Shift

Electromagnetic waves are, independent of the frequency, subject to the Doppler effect. It is however only detectable if there is motion that increases or decreases the distance between the source and the observer. The effect then causes the observed frequency to differ from the radiated frequency of the source.

- If the distance between the source and receiver of electromagnetic waves remains constant, the frequency at the source and the received waves are the same.

Chapter 2. Theoretical Background

- If the distance between the source and receiver of electromagnetic waves is increasing, the frequency at the source and the received waves appear to be lower than the actual frequency of the source wave. Each time the source has completed a wave, it has also moved farther away from the receiver, so the waves arrive less frequently.
- If the distance is decreasing, the frequency of the received wave appears raised relative to the actual transmission frequency (Fig. 2.1). Since the source is getting closer, the waves arrive more frequently.

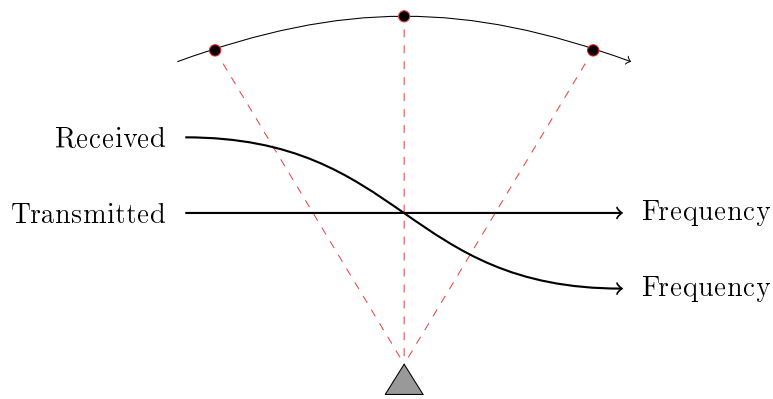


Figure 2.1.: Example of a Doppler shift for a received signal

In the case of a tracked spacecraft by an Earth tracking station both the Earth and the spacecraft are moving through space. If a spacecraft is approaching, orbiting or departing a planetary body, the gravitational attraction of the body is changing the velocity and the trajectory of the spacecraft. If relativistic effects (i.e. special relativity) are neglected, the detectable change in the frequency of the transmitted signal is caused by the Doppler effect. The frequency shift can be expressed by

$$\Delta f = \pm f_0 \frac{\Delta \dot{r}}{c}, \quad (2.1)$$

where Δf is the frequency shift, f_0 is the emitting frequency and the term $\Delta \dot{r}$ is the velocity of the receiver relative to the source: it is positive when the satellite is moving towards the tracking station. c is the propagation velocity of waves in a medium.

Doppler data can be obtained in different tracking modes. When the measured signal originates on a orbiting spacecraft, the resulting Doppler data is called 1-way Doppler data. In this case the spacecraft must be equipped with a precision oscillator on board to achieve an accurate measurement. An alternative is, that the signal is generated by a transmitter on the Earth, which is received and then returned by a spacecraft. When the signal is transmitted and received by the same station, the measurement is referred

Chapter 2. Theoretical Background

to as a 2-way Doppler measurement. If the transmitting and receiving stations differ, the measurement is a 3-way Doppler measurement (Fig. 2.2). When the spacecraft has the capability to operate in the coherent mode, the received signal is multiplied by a turn-around ratio and sent back. That means that the precision is not limited by the stability of the equipment on board of the spacecraft. It is only dependent on the frequency stability of the tracking stations.

In order to achieve precise measurements, the transmitting time and transmitting frequency have to be known. To identify the associated frequency at the receiver more easily, a technique called ramping can be implemented. When a frequency is ramped, it is varied linearly starting with a known initial frequency, at a known rate of frequency change over time (Turyshev and Toth, 2006).

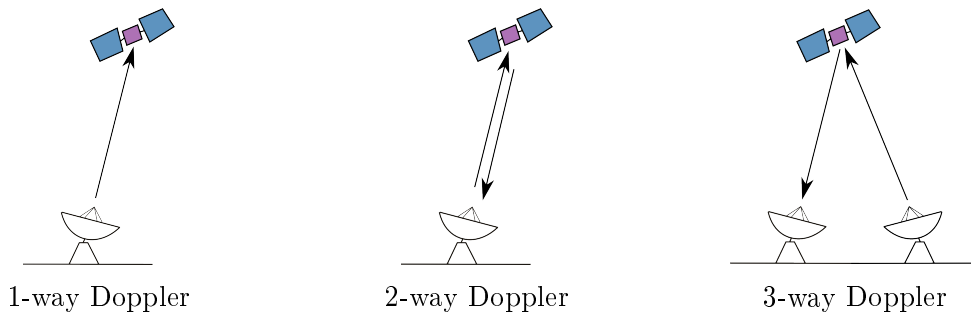


Figure 2.2.: 1-, 2- and 3-way Doppler measurements

2.1.2. Observation Principle

Doppler data is obtained by differentiating the received signal frequency with the station reference frequency. A so called Doppler counter measures the total phase change of a cycle during a count time. According to Thornton and Border (2000) each time the phase of the transmitted signal slips one cycle relative to the phase of the transmitted signal, the distance over which the signal has propagated has increased by one wavelength. The Doppler count thus provides a measure of range over the count time (Fig. 2.3). The precision to which these measurements can be carried out is a function of the received signal strength and station electronics (Turyshev and Toth, 2006).

As already mentioned, there are different tracking modes. The most accurate Doppler measurements can be observed via a 2-way Doppler tracking, where the transmitting and receiving station and therefore the frequency standards are the same.

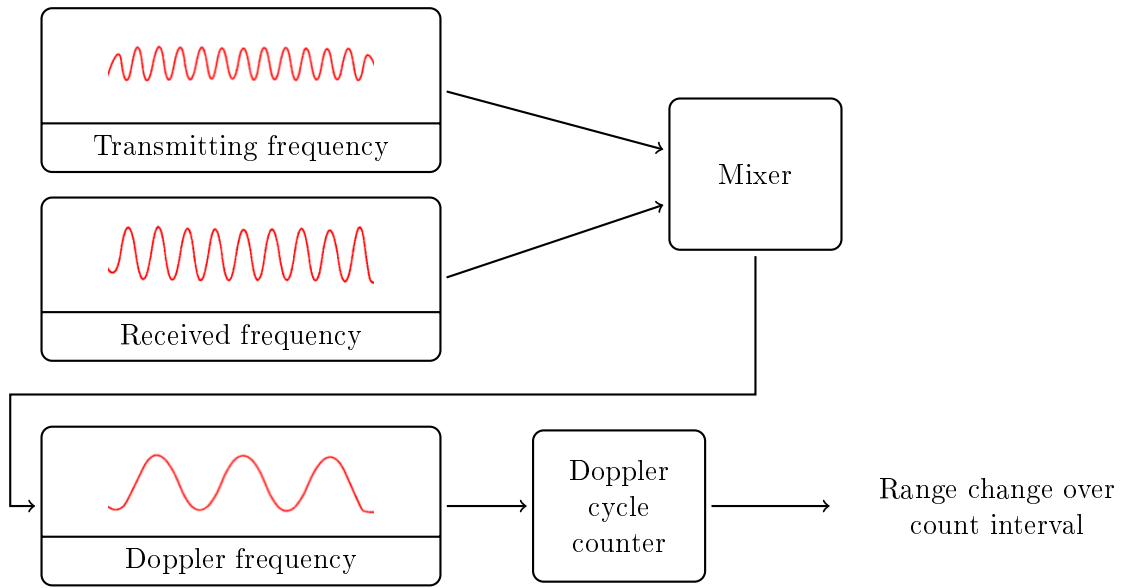


Figure 2.3.: Doppler extraction process
[Adapted from Thornton and Border (2000)]

2.1.2.1. Influences Acting on the Observable

A number of different effects limit the accuracy of Doppler observations. In the following section, the major influence sources are briefly discussed.

- **Clock Instability**
Clock instability is a fundamental source of error in the Doppler extraction process (Fig. 2.3). The received and local reference frequency are mixed together. If there is any offset of the reference frequency from the actual transmitted frequency, this will translate into a range error.
- **Instrumental Effects**
Instruments have to satisfy a lot of different requirements. This limiting factor results in random and systematic measurement errors. Random errors are caused by thermal noise, while systematic errors arise, for example, by instrumental delays and antenna multipath.
- **Transmission Media**
Transmitted radio signals pass on their way to and from the spacecraft the troposphere and the ionosphere of the Earth. Due to the propagation through these regions of the Earth's atmosphere, the frequency of the signal is affected.

In the ionosphere charged particles delay the propagation. The magnitude of the ionospheric error highly depends on the time of the measurement relative to the

Chapter 2. Theoretical Background

Sun cycle, as well as the signal path relative to the Sun. It should be noted that the error is so small that it can be neglected.

The troposphere is a non-dispersive media, i.e. the refraction is independent of the frequency. The effect on the propagation is mainly dependent on the temperature, atmosphere and partial pressure of the water vapour.

2.1.3. Tracking

Doppler data is typically recorded continuously during a tracking pass. In the case of an Earth orbiting satellite, the spacecraft can be tracked from different stations. However, in the interplanetary case, there are only a few dedicated tracking networks.

Due to the requirements for interplanetary missions, the spacecraft gets tracked only by one station at the same time. Meaning that there is just one observation per epoch. To determine an accurate orbit the obtained data must be carefully modelled to take geometry, frequencies, spacecraft delays, relativistic and other effects into account.

2.2. Orbit Determination

A minimum of six elements, for example position and velocity vectors, completely define the orbit of a satellite at one epoch. The method of determining the position and velocity (i.e. the state vector) of an orbiting object is called satellite orbit determination. This object can either be an Earth-orbiting satellite or an interplanetary spacecraft.

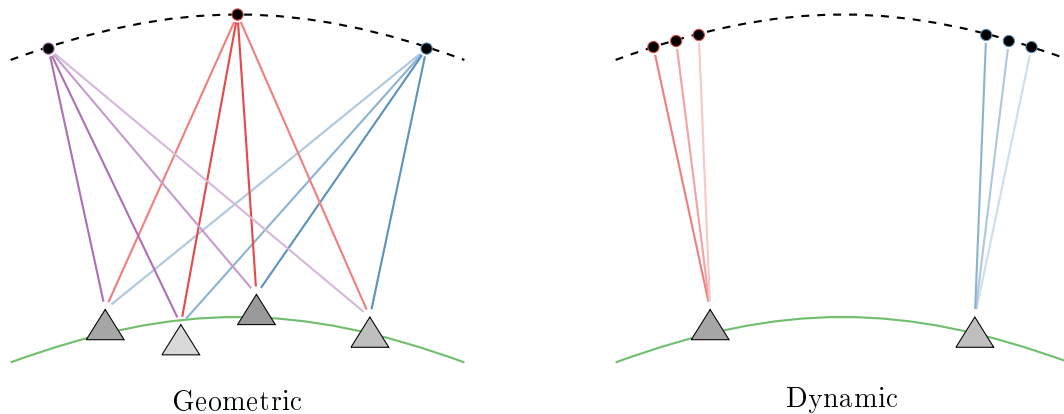


Figure 2.4.: Orbit determination approaches

Chapter 2. Theoretical Background

The main approaches to solve the orbit determination problem are: the geometric or kinematic approach and the dynamic approach (Fig. 2.4). The kinematic approach is purely geometric and uses no dynamical description of the spacecraft's motion. Instead, the approach relies purely on observation data to estimate the state vectors at each epoch. Therefore, the approach requires a high data sampling as well as the availability of accurate measurements. The dynamic approach, however, uses a dynamical model to describe the motion of the spacecraft, because there is typically just one observation per epoch available. Additionally, all forces acting on the spacecraft have to be modelled and/or parametrized. The accuracy is mostly limited by modelling errors (Hobbs and Bohn, 2006, Bae, 2006).

Due to the situation that the orbit of the spacecraft tracked with Doppler data has just one observation per epoch, the dynamic approach has to be used. The dynamic orbit determination is a differential-correction i.e. non-linear least squares technique. It can accurately estimate the orbit's state from measurements.

The satellite's motion can be described mathematically by a set of equation of motions

$$\ddot{\mathbf{r}} = \frac{GM}{r^3} \cdot \mathbf{r} + f_G(\mathbf{r}) + f_{NG}(\mathbf{r}, \dot{\mathbf{r}}), \quad (2.2)$$

where \mathbf{r} is the state vector of the satellite. The term f_{NG} is the sum of all non-gravitational accelerations acting on the satellite, f_G is the sum of gravitational forces acting on the satellite, which are both dependent on the position. The non-gravitational force drag is also dependent on the velocity.

The orbit determination procedure comprises of an iterative adjustment of trajectory parameters and model parameters. Starting from given a priori conditions, the equation of motion is numerically integrated. Residuals are obtained by differencing the observations and modelled measurements. By a least-squares adjustment corrections to the a priori parameters can be determined. Due to the non-linear problem, multiple iterations are required to achieve convergence.

The assumption is that at each time t_i a sensor observed a range and range-rate, so that

$$y_{0_i} = f \left(\begin{bmatrix} \mathbf{r}_0 \\ \dot{\mathbf{r}}_0 \end{bmatrix}_{t_i} \right). \quad (2.3)$$

To calculate residuals, predicted measurements have to be computed from the position and velocity vectors:

$$y_{c_i} = f \left(\begin{bmatrix} \mathbf{r}_c \\ \dot{\mathbf{r}}_c \end{bmatrix}_{t_i} \right). \quad (2.4)$$

y_{c_i} is a non-linear function of the position, the velocity and time. To estimate the position vectors \mathbf{r}_i and the velocity vectors $\dot{\mathbf{r}}_i$, the residuals ε_i are needed for the least-squares adjustment:

$$\varepsilon_i = y_{0_i} - y_{c_i}. \quad (2.5)$$

The aim is to correct the parameters of the trajectory in such a way that the difference between the observed and computed measurements are minimal. To obtain the optimal solution the orbit determination problem is iterated till a minimum is reached.

2.2.1. Forces Acting on a Satellite

The primary force acting on a spacecraft in space are gravitational attractions of planetary bodies. The bodies can be treated as Newtonian point masses as long as the spacecraft is far from these bodies. When the spacecraft is in the vicinity of a planetary body, corrections due the general relativity, oblateness as well as the mass distribution must be considered. Also, the gravitational forces of other planetary bodies have an effect on the central body the satellite is orbiting. The lunar body tides are for example caused by the gravitational interaction between the Earth and the Moon and affect hence the spacecraft as well.

The trajectory of a spacecraft is also modified by non-gravitational forces. Non-gravitational forces are, for example, solar radiation pressure, atmospheric drag and other effects like the albedo acting on a spacecraft. These forces are functions of the position of the satellite relative to the planets, and of the Sun and Moon relative to the Earth. Only the atmospheric drag is additionally a function of the relative satellite velocity with respect to the atmosphere.

Additionally, manoeuvres are necessary to establish and maintain the target orbit, and to prevent impacts due to natural orbit evolution (Ryne et al., 2013).

2.3. Time and Reference Systems

In the process of analysing data from RS measurements, various time and coordinate systems and frames are necessary. Also, the transformation between the different frames

Chapter 2. Theoretical Background

is of great significance to obtain accurate results. The used frames and transformations are described in the following sections. For more information see the International Earth Rotation and Reference Systems Service ([IERS](#)) Conventions 2010 ([Petit and Luzum, 2010](#)).

2.3.1. Time Scales

The position of the spacecraft and the receiving tracking station on Earth has to be known very precisely in different time systems. While the position of a planetary body is w.r.t. to the Ephemeris Time ([ET](#)), the recorded data as well as the station positions are referenced to the Coordinated Universal Time ([UTC](#)).

2.3.1.1. Ephemeris Time

[ET](#) is a relativistic coordinate time scale. It is the independent variable for the motion of celestial bodies, spacecraft, and light rays ([Moyer, 2000](#)). It can be expressed in the form of Barycentric Dynamic Time ([TDB](#)) or Terrestrial Dynamic Time ([TDT](#)).

2.3.1.2. Coordinated Universal Time

Universal Time ([UT](#)) is the basis for all civil time-keeping. It is an observed time scale w.r.t. the Earth's rotation and therefore not uniform.

[UTC](#) is a uniform time scale that approximates [UT](#). It is kept within 9s to [UT](#) by introducing leap seconds. This is why it is synchronous with the International Atomic Time ([TAI](#)), but an integer number of seconds behind.

2.3.1.3. International Atomic Time

[TAI](#) is based upon the seconds unit of the [SI](#) second and obtained from a worldwide system of synchronized atomic clocks. It is the basis for the [UTC](#) and the [ET](#).

2.3.2. Time Differences

2.3.2.1. TAI - UT

As previously mentioned, the time difference **TAI - UTC** is an integer number of leap seconds. Its value is time dependent. The decision to introduce a leap second in **UTC** is the responsibility of the **IERS**¹.

2.3.2.2. ET - TAI

In the geocentric frame of reference the difference between the **ET** and **TAI** can be approximated by

$$\Delta\text{ET} = \text{ET} - \text{TAI} = 32.184 \text{ s.} \quad (2.6)$$

In the barycentric frame of reference the relativistic effects have to be included:

$$\begin{aligned} \Delta\text{ET} = \text{ET} - \text{TAI} = & 32.184 \text{ s} + \frac{2}{c^2}(\dot{\mathbf{r}}_B^S \cdot \mathbf{r}_B^S) + \frac{1}{c^2}(\dot{\mathbf{r}}_B^C \cdot \mathbf{r}_E^B) + \frac{1}{c^2}(\dot{\mathbf{r}}_E^C \cdot \mathbf{r}_A^E) \\ & + \frac{\gamma_J}{c^2(\gamma_S + \gamma_J)}(\dot{\mathbf{r}}_J^S \cdot \mathbf{r}_J^S) + \frac{\gamma_{\text{Sa}}}{c^2(\gamma_S + \gamma_{\text{Sa}})}(\dot{\mathbf{r}}_{\text{Sa}}^S \cdot \mathbf{r}_{\text{Sa}}^S) \\ & + \frac{1}{c^2}(\dot{\mathbf{r}}_S^C \cdot \mathbf{r}_B^S), \end{aligned} \quad (2.7)$$

where \mathbf{r}_j^i and $\dot{\mathbf{r}}_j^i$ are the space-fixed position and velocity vectors of point i relative to point j . The indices indicate the solar-system barycentre (C), the sun (S), the Earth-Moon barycentre (B), the Earth (E), the Moon (M), Jupiter (J), Saturn (Sa), and the location of the tracking station on Earth (A). γ_S , γ_J and γ_{Sa} are the gravitational constants of the Sun, Jupiter and Saturn, while c is the speed of light (Moyer, 2000).

2.3.3. Reference Systems

For an accurate determination of the calculated observable the coordinate systems as well as the transformation play a crucial part. The tracking station coordinates are given in the **ITRF** (e.g. Folkner (1997)), the **GRAIL** coordinates are provided in an inertial, Moon-centred system, while the ephemeris of the planetary bodies are in the solar-system barycentric system. To supply all coordinates in the same system, various

¹Bulletin 3: <http://hpiers.obspm.fr/eop-pc/index.php?index=bulletins&lang=en>

Chapter 2. Theoretical Background

transformations are needed. In the following sections, the used systems and transformations are briefly described.

2.3.3.1. ITRF

According to the definition of the [IERS](#), the International Terrestrial Reference System ([ITRS](#)) is specified as geocentric, with its origin being the center of mass for the Earth, including oceans and atmosphere. A triplet of right-handed, orthogonal vectors express the orientation of the system emerging from the origin. The system co-rotates with the Earth. Meaning that the position of a point undergoes only small variations with time.

The International Terrestrial Reference Frame ([ITRF](#)) is a realization of the theoretical description of the [ITRS](#) by the [IERS](#). Up to this point twelve versions of the [ITRF](#) have been published. Each of the realizations superseded its predecessor. With the available transformation parameters, coordinates can be transformed via a Helmert transformation (also called a seven-parameter transformation) between the reference frames (Eq. 2.8):

$$\mathbf{r}' = \mathbf{r} + \mathbf{t} + \mu \mathbf{R}(\alpha_{1,2,3}) \mathbf{r} \quad (2.8)$$

where \mathbf{r}' is the transformed vector, while \mathbf{r} is the initial vector. The parameters are the translation vector \mathbf{t} , the scale factor μ and the rotation matrix $\mathbf{R}(\alpha_{1,2,3})$ (Eq. 2.9).

$$\mathbf{R}(\alpha_{1,2,3}) = \begin{bmatrix} 0 & -\alpha_3 & \alpha_2 \\ \alpha_3 & 0 & -\alpha_1 \\ -\alpha_2 & \alpha_1 & 0 \end{bmatrix} \quad (2.9)$$

2.3.3.2. ICRF

The International Celestial Reference System ([ICRS](#)) consists of a Barycentric Celestial Reference System ([BCRS](#)) and a Geocentric Celestial Reference System ([GCRS](#)). The International Celestial Reference Frame ([ICRF](#)) is a realization of the theoretical description of the [ICRS](#). It is realised by precise J2000.0 equatorial coordinates of extragalactic radio sources observed with Very Long Baseline Interferometry ([VLBI](#)). Continuous maintenance is necessary to ensure that the reference directions are fixed.

A triplet of right-handed, orthogonal vectors express the orientation of the system emerging from the origin. The axis directions are fixed with respect to the distant matter of the universe. While the origin of the [GCRS](#) is the geocenter, the origin of the [BCRS](#)

Chapter 2. Theoretical Background

is the barycentre. The lunar celestial reference system is the **GCRS** shifted to the center of the Moon. It also refers to the inertial mean ecliptic at the fundamental epoch J2000.0.

2.3.3.3. ITRF - ICRF

The transformation to relate the **ITRF** and **ICRF** can be written in short as

$$\mathbf{r}_{\text{ICRF}} = \mathbf{Q}(t) \cdot \mathbf{R}(t) \cdot \mathbf{W}(t) \cdot \mathbf{r}_{\text{ITRF}}, \quad (2.10)$$

where \mathbf{r}_{ICRF} denotes the position vector in the **ICRF**, and \mathbf{r}_{ITRF} describes the position vector in the **ITRF**. $\mathbf{Q}(t)$ is the transformation matrix arising due to precession and nutation. The matrix $\mathbf{R}(t)$ deals with the rotation of the Earth around its rotation axis, while $\mathbf{W}(t)$ arises from the polar motion i.e. the change of the Earth's rotation vector relative to the Earth's body.

Chapter 3.

GRAIL Mission

The [GRAIL](#) mission of the [NASA](#) Discovery Program was comprised of two spacecraft flying in a low altitude polar orbit around the Moon (Fig. 3.1). The mission's objective was to measure the lunar gravity field in order to help answer fundamental questions about the Moon's internal structure, thermal evolution and collisional history.

The twin [GRAIL](#) spacecraft, [GRAIL-A](#) and [GRAIL-B](#), were launched on 10 September 2011 at the Cape Canaveral Air Force Station, Florida ([You et al., 2012](#)). Individually they arrived at the Moon on 31 December 2011 and on 1 January 2012. The three-month primary mission of gravity mapping began on 1 March 2012 and ended on 29 May 2012 ([Konopliv et al., 2013](#)). [NASA](#) approved an extended [GRAIL](#) mission until December 2012.

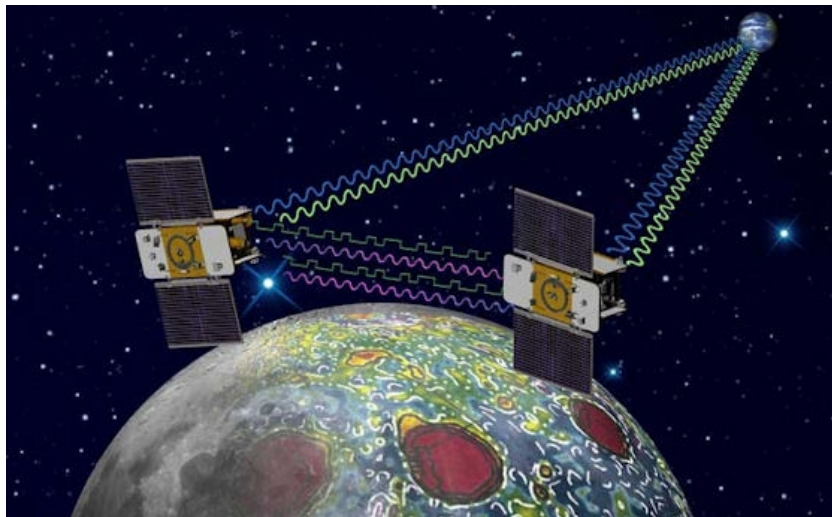


Figure 3.1.: GRAIL mission ©NASA/JPL-Caltech

3.1. Orbit

The main goal of the primary mission was to collect gravity data. The used orbit had to satisfy scientific requirements, as well as practical and technical restraints. The orbit was selected in such a way, that there weren't any manoeuvres required to maintain it.

The primary design parameter from the scientific perspective was the orbit altitude, since the sensitivity to the lunar gravity field decreases with the distance to the body. The altitude was limited due to life time constraints. Another factor was the goal of a global coverage. Therefore the used orbit was a near-polar, near-circular orbit with an altitude of 55 km. During the three-month primary mission the moon rotated three times underneath the [GRAIL](#) orbit ([NASA, 2011](#)). The extended mission permitted a second three-month phase at an average altitude of 23 km. Due to the low orbit, the resolution of the gravity field measurements could be increased by a factor of two ([Zuber et al., 2013a](#)).

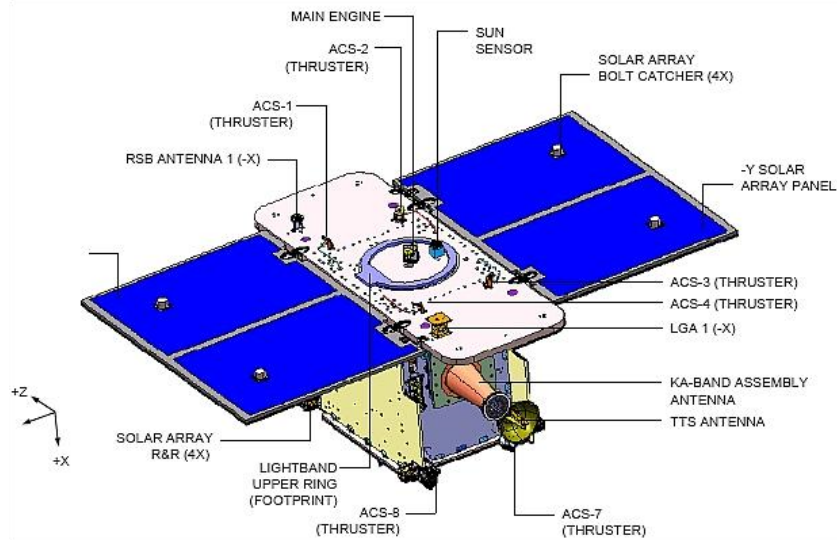


Figure 3.2.: Top view of the GRAIL spacecraft ©NASA, LMSSC

3.2. Spacecraft

The two [GRAIL](#) spacecraft were nearly identical. The few important differences were due to the need to point to each other during the science missions. Therefore, the star trackers and the lunar gravity ranging system were mounted differently. Also the orientation of the orbiters was different. They flew facing each other, so that the Ka-band antenna could point to each other (Fig. 3.2).

The main structure of the spacecraft was about the size of a washing machine, with a mass of about 200 kg. The attitude was controlled by a sun sensor, a star tracker, reaction wheels and an inertial measurement unit. The solar array panels, with a total cell area of 2.8 m², supplied the necessary power (Kahan, 2009).

3.3. Ranging System

Communication between Earth and spacecraft were made within internationally allocated frequency bands. The ranging system instruments on board of GRAIL generated radio signals at Ka-band, X-band and S-band (Table 3.1). The Ka-band signal for ranging and S-band signal for the time transfer were transmitted and measured between the twin spacecraft (Fig. 3.1). The communication to and from Earth was transmitted with the S-band. To determine the spacecraft trajectories, 1-way Doppler (X-band) and 2-way Doppler (S-band) data was measured and stored in so called Orbit Data Files (ODF) (Konopliv et al., 2013, Kahan, 2013).

Band	Uplink Frequency [MHz]	Downlink Frequency [MHz]
S	2110 - 2120	2290 - 2300
X	7145 - 7190	8400 - 8450
Ka	34200 - 34700	31800 - 32300

Table 3.1.: Uplink and downlink frequencies for DSN (Thornton and Border, 2000)

To improve the ability to achieve and maintain lock, the radio signal was "ramped", which means that instead of an constant frequency, a continuous linearly increasing and decreasing frequency was used. In the 2-way mode, the received frequency at the satellite was multiplied with a turn-around ratio (Table 3.2) and then sent back to the tracking station. This so-called coherent modus has the advantage that the spacecraft does not need to have a highly stable oscillator.

Uplink Band	Downlink Band	S	X	Ka
S		240/221	880/221	3344/221
K		240/749	880/749	3344/749
Ka		240/3599	880/3599	3344/3599

Table 3.2.: Turn-around ratios (Moyer, 2000)

3.4. Tracking Network

GRAIL was tracked by the DSN. The DSN is comprised by three Deep Space Station (DSS) facilities in Goldstone (USA), Canberra (Australia) and Madrid (Spain) (Fig. 3.3). Due to the spatial distribution of the complexes - approximately 120 degrees of longitude are between them - it is possible to constantly observe a spacecraft. Each of the complexes is equipped with large antennas of different sizes (Table 3.3). The coordinates of the DSN station locations and their velocities can be found in Tables 3.4 and 3.5.

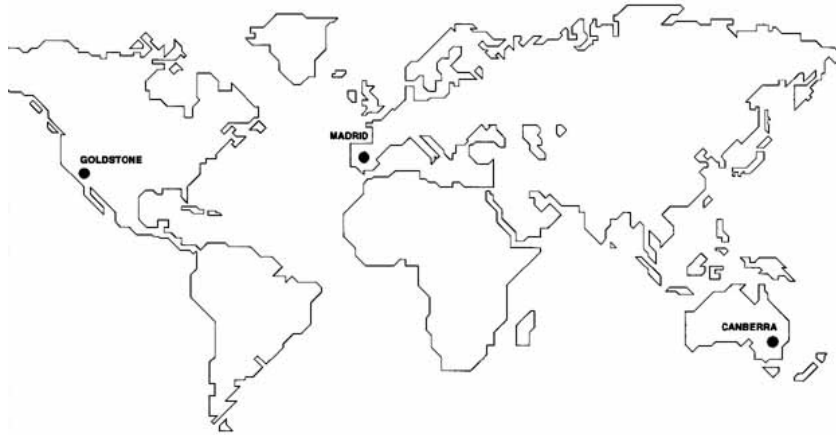


Figure 3.3.: Global distribution of DSN ©NASA/JPL-Caltech

Station	Complex	Station Type	GRAIL Band
DSS-24	Goldstone	34 m Beam Wave Guide	S, X
DSS-27	Goldstone	34 m Beam Wave Guide	S
DSS-34	Canberra	34 m Beam Wave Guide	S, X
DSS-45	Canberra	34 m High Efficiency	S, X
DSS-54	Madrid	34 m Beam Wave Guide	S, X
DSS-65	Madrid	34 m High Efficiency	S, X

Table 3.3.: DSN tracking stations supporting GRAIL (Ryne et al., 2013)

The main task of the DSN is to radiate commands and receive telemetry data from active spacecraft. Thus, ground stations have the ability to transmit waveforms which can be echoed by distant spacecraft. The transmission and reception is possible in several radio-frequency bands (Table 3.1).

Station	X-Coordinate [m]	Y-Coordinate [m]	Z-Coordinate [m]
DSS-24	-2354906.495	-4646840.128	3669242.317
DSS-27	-2349915.260	-4656756.484	3660096.529
DSS-34	-4461146.756	2682439.293	-3674393.542
DSS-45	-4460935.250	2682765.710	-3674381.402
DSS-54	4849519.988	-360641.653	4114504.590
DSS-65	4849336.730	-360488.859	4114748.775

Table 3.4.: Coordinates of the primary DSN tracking stations (Slobin, 2014)
[ITRF93, epoch 1993.00]

Complex	X-Velocity [m/yr]	Y-Velocity [m/yr]	Z-Velocity [m/yr]	Remark
Goldstone	0.0180	0.0065	0.0038	Stations No. 1x to 2x
Canberra	0.0335	0.0041	0.0392	Stations No. 3x to 4x
Madrid	0.0100	0.0242	0.0156	Stations No. 5x to 6x

Table 3.5.: Site velocities for DSS (Slobin, 2014)

Chapter 4.

Data

In section 2.1.2 the observation principle was already described generally. This chapter focusses on the actual observation, its modelling and its storage.

4.1. Observable

As already mentioned in section 3.3, the DSN stores the observable in ODFs. The Doppler observable (Items 4 and 5 in Table 4.2), provided in the files, represents the average frequency change during a given time interval, rather than the actual measurements made at the DSN. The time tag t_r (Items 1 and 2 in Table 4.2) is in the midpoint of the counting (i.e. Doppler) interval or compression time (Item 20 in Table 4.2). The start of the interval t_i is the time tag minus half of the compression time, and the end of the interval t_j is the time tag plus half of the compression time.

The Doppler observable is computed according to DSN (2013) by the following equation

$$Observable = \frac{B}{|B|} \cdot \left[\frac{N_j - N_i}{t_j - t_i} - |f_b \cdot K + N| \right], \quad (4.1)$$

where B is the bias placed on the receiver, N_i and N_j are the Doppler counts at the corresponding time t_i and t_j , respectively. K is the spacecraft turn-around ratio, which varies with the used band (Table 3.2). The frequency f_b is a combination of the following quantities for 1-way Doppler data

$$f_b = \frac{X_1}{X_2} \cdot (X_3 \cdot f_r + X_4) - f_{sc} \quad (4.2)$$

and for all other Doppler data

$$f_b = \frac{X_1}{X_2} \cdot (X_3 \cdot f_r + X_4) - \frac{T_1}{T_2} \cdot (T_3 \cdot f_t + T_4), \quad (4.3)$$

where f_r is the receiver frequency at time t_r and f_t is the transmitter frequency at time t_r minus the round trip light time. f_{sc} is the spacecraft frequency. The values X_i and T_i are values corresponding to the used band links (Item 12 - 14 in Table 4.2) and can be found in the meta data file of the ODF in the PDS (DSN, 2013, Kwok, 2008).

In the case of the GRAIL 2-way Doppler data, the transmitted frequency f_t is ramped. As already mentioned when a frequency is ramped, it is varied linearly starting with a known initial frequency at a known rate of frequency change over time. According to Liu (1973) a unique correspondence between time of transmission and frequency of transmission is established by ramping the transmitted frequency. Comparison of the time and frequency of reception to the transmitted frequency value and time allows to associate the quantities. There is no difference in the observation process. However, when calculating the observable the frequency has to be ramped according to the ramp information at the transmitting time.

4.2. Data Formats

The tracking stations of the DSN store the measured observations in Orbit Data Files (ODF). Together with the meteorological information in the WEA format, the computed observable, i.e. range-rate, can be determined. The following section details the different data formats.

4.2.1. ODF Tracking Data Format

The format and content of the ODFs are specified in the ODF interface. This TRK-2-18 ODF format is used for radio metric data observed by the DSN. Its format documentation is available at the PDS by NASA.

An ODF is a binary file and consists of radio metric data for one spacecraft and one or more stations. The file is divided into seven groups of different information (Table 4.1), distinguishable by the primary key in the header. Groups 1-6 contain a header, which contains the group identification, and data, which contains information. The "End-of-File Group" is made up of a header only. Within the groups, the header or data is stored in 36 byte blocks. An ODF is composed of an integer multiple of 8064 byte. If the file contains less than an integer multiple, the remaining space gets filled with filler bytes (Kwok, 2008).

Chapter 4. Data

No.	Byte	Name	Comment
1		36 File Label Group Header Primary Key = 101	Required
		36 File Label Group Data	
2		36 Identifier Group Header Primary Key = 107	Required
		36 Identifier Group Data	
3	36*(1+N)	36 Orbit Data Group Header Primary Key = 109	Required, Multiple, 1 Header for All Data
		Orbit Data Group Data No. of Data Blocks = N	
4	36*(1+M+L)	36 Ramp Group Header Primary Key = 2030	Optional, Multiple, 1 Header for All Data
		Ramp Group Data No. of DSS = M, No. of Data Blocks = L	
5	36*(1+B)	36 Clock Offset Group Header Primary Key = 2040	Optional, Multiple, 1 Header for All Data
		Clock Offset Group Data No. of Data Blocks = B	
6	36*(1+D)	36 Data Summary Group Header Primary Key = 105	Optional, Multiple, 1 Header for All Data
		Data Summary Group Data No. of Data Blocks = D	
7		36 End-of-File Group Header Primary Key = -1	Required, Header only
		Filler Bytes	

Table 4.1.: ODF layout (Kwok, 2008)

Chapter 4. Data

The "File Label Group" is the first record. It identifies the spacecraft, the file creation time, the hardware and the software associated with the ODF. The ID number for the spacecraft is specified in DSN document OPS-6-8. In the case of GRAIL, the ID number is 177 for GRAIL-A and 181 for GRAIL-B. The "Identifier Group" is usually the second record. It is sometimes used to identify contents of data records that follow.

The "Orbit Data Group" is the third record group. It contains the majority of the data included in the file. Within the Orbit Data Group block there is usually just one header. The subsequent observation records (Table 4.2) are ordered by time. An observation record contains a time stamp, station and satellite IDs as well as frequency and compression time. Data types are distinguished through their data type values. Regarding GRAIL, the used data types are 1-way Doppler (11), 2-way Doppler (12), 3-way Doppler (13) and the range observable (37).

"Ramp Groups" are the fourth record group. They contain information referring to the tuning of receivers or transmitters. There is usually one Ramp Group for each DSN station. The information covers time stamp, ramp rate as well as ramp start and end frequency (Table 4.3).

The End-of-File Group is the last record group. In the case of GRAIL, it is the fifth record group and denotes the end of the file.

Listing 4.1 shows an example of an ODF file converted to an ASCII file. In contrast to Tables 4.2 and 4.3, which describe how exactly the information is stored in the ODF, the integer and fractional parts of quantities are already combined. The commentary lines with hyphens and blanks contains group information. Additionally some quantities are outlined in the text as well as in the listing in the same color to allow an easier understanding.

After the first line with the primary key 101, the second line contains the spacecraft ID and the reference time. After the primary key 109 the observation data follows. The first information in the Table is the time information in seconds since the reference time. The station delay in nanoseconds and observation information in Hertz follow in the list. The next interesting information are the transmitting and receiving station IDs and the measurement type. It can be seen, that the displayed data is 1-way and 2-way Doppler data tracked by the DSS 45. Afterwards the used band links are detailed. Next, the satellite ID, which is in the case of GRAIL 177, and the reference frequency follow. Lastly, the counting interval (i.e. Doppler interval) is given.

The ramp information is marked by the primary key 2030. The time tags are the ramp start time and the ramp end time. The second quantity given is the ramp rate in Hertz per second. The last important informations are the ramp start frequency, which is needed to compute the ramped frequency and the tracking station ID to specify for which station the ramp information applies.

Listing 4.1: ODF file

```

----- Label Group -----
 101 0 1 0
TDDS AMMOS 177 1120307 233848 19500101 000000

----- Identifier Group -----
 107 0 1 2
TIMETAG OBSRVBL 177 1120307 233848 19500101 000000
FREQ, ANCILLARY-DATA

----- Orbit Data Group -----
 109 0 1 4
1961920960.000 0 374.999647617 2 45 45 0 12 1 1 1 0 4 177 1 2099067282000 0 100 0
1961920960.000 0 -42098.121376990 2 45 0 0 11 2 0 1 0 3 177 1 2304981818181 0 100 0
1961920961.000 0 380.031273365 2 45 45 0 12 1 1 1 0 4 177 1 2099067282000 0 100 0
1961920961.000 0 -42081.119548797 2 45 0 0 11 2 0 1 0 3 177 1 2304981818181 0 100 0
1961920962.000 0 384.709175587 2 45 45 0 12 1 1 1 0 4 177 1 2099067282000 0 100 0
1961920962.000 0 -42064.053752898 2 45 0 0 11 2 0 1 0 3 177 1 2304981818181 0 100 0
1961920963.000 0 388.874752522 2 45 45 0 12 1 1 1 0 4 177 1 2099067282000 0 100 0
1961920963.000 0 -42046.983613967 2 45 0 0 11 2 0 1 0 3 177 1 2304981818181 0 100 0

----- Ramp Groups -----
 2030 45 1 93128
1961920223.000 -2.042720 2099045453.12618 45 1961920316.000
1961920316.000 -1.230140 2099045263.15322 45 1961920407.000
1961920407.000 -0.400610 2099045151.21048 45 1961920500.000
1961920500.000 0.439330 2099045113.95375 45 1961920591.000
1961920591.000 1.280430 2099045153.93278 45 1961920682.000
1961920682.000 2.128200 2099045270.45191 45 1961920774.000
1961920774.000 2.976690 2099045466.24631 45 1961920793.000
1961920793.000 35002.976730 2099045522.80342 45 1961920795.000

----- End of File Group -----
-1 0 0 93930

```

Chapter 4. Data

No.	Start-Bit	Bits	Name	Unit/Value
1	0	32	Record Time Tag Integer Part	Seconds Since 0 hours UTC on 1.1.1950
2	32	10	Record Time Tag Fractional Part	Milliseconds
3	42	22	Receiving Station Downlink Delay	Nanoseconds
4	64	32	Observable Integer Part	Hertz See Section 4.1
5	96	32	Observable Fractional Part	Hertz Scaled by 10^{-9}
6	128	3	Format ID	2 if document cre- ated after 14.4.1997
7	131	7	Receiving Station ID	
8	138	7	Transmitting Station ID	
9	145	2	Network ID	0=DSN Block V
10	147	6	Data Type	1x = x-way Doppler
11	153	2	Downlink Band ID	1 = S-Band
12	155	2	Uplink Band ID	1 = S-Band
13	157	2	ExciterBand ID	1 = S-Band
14	159	1	Data Validity Indicator	0 = good
15	160	7	Second Receiving Station	
16	167	10	Spacecraft ID	
17	177	1	Receiver/Exciter Independent Flag	
18	178	46	Reference Frequency	Millihertz
29	224	20	Train Axis Angle	Millidegrees
20	244	22	Compression Time	0.01 Seconds
21	266	22	Transmitting Station Uplink Delay	Seconds

Table 4.2.: ODF orbit data group (Kwok, 2008)

Chapter 4. Data

No.	Start-Bit	Bits	Name	Unit
1	0	32	Ramp Start Time Tag Integer Part	Seconds Since 0 hours UTC on 1.1.1950
2	32	32	Ramp Start Time Tag Fractional Part	Nanoseconds
3	64	32	Ramp Rate Integer Part	Hertz per Second
4	96	32	Ramp Rate Fractional Part	Nanohertz per Second
5	138	22	Ramp Start Frequency	Gigahertz
6	160	10	Transmitting/Receiving Station ID Number	
7	170	32	Ramp Start Frequency Integer Part	Hertz
8	202	32	Ramp Start Frequency Fractional Part	Nanohertz
9	234	32	Ramp End Frequency Integer Part	Hertz
10	266	32	Ramp End Frequency Fractional Part	Nanohertz

Table 4.3.: ODF ramp data group (Kwok, 2008)

Character	Item	Format
1-5	Date	DATE
7-12	Two Digit Integer Year, Month and Day	YYMMDD
14-17	Day of Year	Day of Year (DOY)
19-21	Three Digit Integer DOY	DDD
23-25	Deep Space Station	DSS
17-29	Two Digit DSS Number	10, 40 or 60

Table 4.4.: WEA header format (Connally, 2006)

Character	Item	Format	Unit
2-5	Time	HHMM	
11-15	Dew Point	STT.T	Degree Celsius
20-24	Ambient Temperature	STT.T	Degree Celsius
29-34	Pressure	PPPP.P	Millibars
40-45	Water Vapor Partial Pressure	PPPP.P	Millibars
55-57	Relative Humidity	PPP	Percent

Table 4.5.: WEA data format (Connally, 2006)

4.2.2. WEA File Format

The format and content of the meteorological data provided by the [DSN](#) is defined in the [DSN Tracking System Interfaces](#), particularly in the Weather Data Interface. The format is called TRK-2-24 and can be found at the [PDS](#) by [NASA](#).

The weather information at the Deep Space Stations ([DSS](#)) is recorded at a one-minute rate and thinned to a nominal sampling interval of 30 minutes. A typical file covers one calendar year for one [DSS](#). The weather data is provided in the form of line orientated text files in [ASCII](#) format.

Each day's data is preceded by a five line header. The first line consists of the date, [DOY](#) and the [DSS](#). The second line is blank. The third and fourth lines consist of column titles and units of measurement describing the data in each column ([Table 4.4](#)). The fifth line consists of hyphens and blanks to separate the header from the data.

In the data section each data line comprises of a time tag in hours and minutes in [UTC](#) and five data fields: namely the dew point, the ambient temperature, pressure, water vapour partial pressure and relative humidity ([Table 4.5](#)). Due to system malfunctions, the number of data lines per day varies. The last data line of each day is followed by a blank line. If there is no data at all for a day, the header will not be in the file either ([Connally, 2006](#)).

[Listing 4.2](#) shows sample data from two consecutive days. In the header, the date and Deep Space Communications Complexes ([DSCC](#)) are stored. In this example, some data from the first day is missing. It is also possible that just some measurements are available, meaning that one or more instruments are working. Then there are blanks in the space of the missing values.

Chapter 4. Data

Listing 4.2: WEA file

DATE: 030121 DOY: 021 DSS 10

TIME (HHMM)	DEW PT (C)	TEMP (C)	PRESSURE (mb)	H2O PARTIAL PRES (mb)	RELATIVE HUM(%)
-----	-----	-----	-----	-----	-----
0000	-3.9	16.9	905.1	4.7	24
0030	-4.1	16.4	905.3	4.6	24
0100	-4.0	15.4	905.4	4.7	26
0130	-4.0	15.1	905.5	4.7	27
2330	-2.7	18.1	905.4	5.1	24
2359	-2.4	17.9	905.5	5.3	25

DATE: 030122 DOY: 022 DSS 10

TIME (HHMM)	DEW PT (C)	TEMP (C)	PRESSURE (mb)	H2O PARTIAL PRES (mb)	RELATIVE HUM(%)
-----	-----	-----	-----	-----	-----
0000	-2.4	17.9	905.5	5.2	25
0030	-1.3	17.1	905.5	5.7	29
0100	-1.3	15.9	905.8	5.7	31

Chapter 5.

Methodology

Figure 5.1 shows a schematic overview of the radio navigation process. As already mentioned the Doppler observable is defined as the difference between the number of cycles received by at tracking station compared the number of cycles produced by a reference frequency during a count interval. The left part of the figure, i.e. the observed observation, was already addressed in chapter 4.

The right part of the figure, i.e. the computed observation, is the subject of this chapter. The Doppler observable can be computed accurately if the orbit of the spacecraft and the position of the tracking station is known. Additionally information on the transmission medium along the signal path is necessary.

As the figure shows, the observation processing is part of of a bigger system. The trajectory can be calculated by using an initial state vector of the spacecraft in combination with models of the forces acting upon the satellite. With the trajectory, ephemeris and correction models the range-rate can be computed. As already detailed in chapter 2 the residuals are input for the least squares adjustment. The model parameters than can be adjusted to achieve a best fit between the model and the observations.

Based on the process of [GEODYN](#), the calculation of the computed observation, i.e. the range-rate, was reconstructed. This chapter discusses the determination method of the observable computation and gives a detailed insight into the implementation.

As per [Turyshchev and Toth \(2006\)](#) a 2-way Doppler data is completely characterized by:

- the location of the transmitting and receiving station,
- the time of reception,
- the length of the Doppler count interval,
- the Doppler count,
- the transmission frequency,

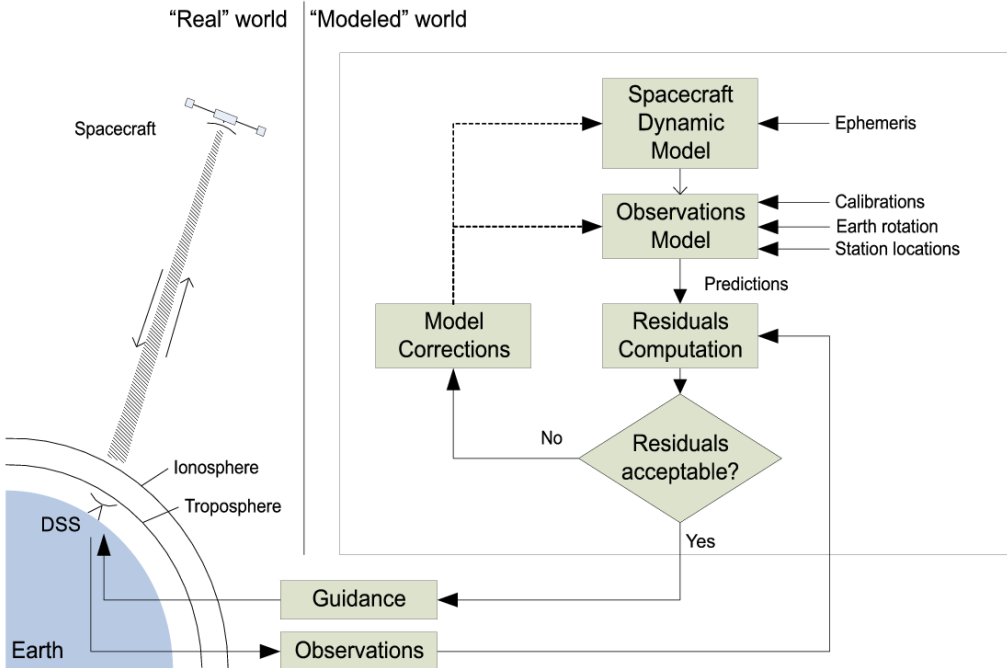


Figure 5.1.: Schematic overview of the radio navigation process (Turyshev and Toth, 2006)

- the reference frequency of the receiver and
- the ramp information.

This information as well as additional meteorological data for the tropospheric correction is part of the computation process. The whole process is summarized in the section 5.5.

5.1. Light Time Solution

The light time solution is implemented according to Moyer (2000) and is the first step to obtain the computed observable. The satellites light time solution can be either realized in the solar system barycentric frame or in the local geocentric frame. It must be noted that the Moon is not close enough to Earth to use the local geocentric frame.

At the beginning only the receiving time t_3 and the coordinates of the tracking station \mathbf{r}_3 at time t_3 are known. The solution produces the reflection time t_2 and the position of the spacecraft \mathbf{r}_2 at time t_2 as well as the transmission time t_1 and the position of the tracking station \mathbf{r}_1 at time t_1 (Fig. 5.2).

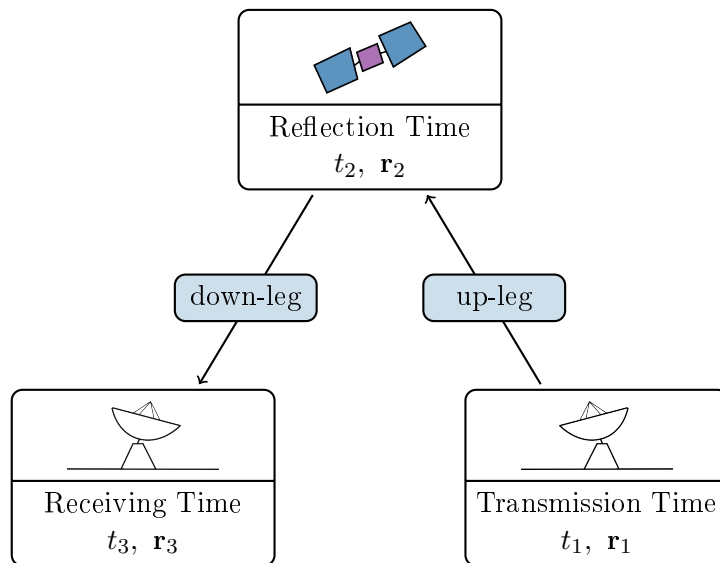


Figure 5.2.: Notation for light time solution

5.1.1. Round Trip Light Time

A 2-way Doppler data comprises of the signal transmitted from the tracking station to the satellite and also the reflected signal from the satellite back to the tracking station.

The signal is measured at the tracking station at the receiving time t_3 at the end of the count interval. The signal was transmitted and reflected back at the reflection time t_2 or $t_3 - \tau_{\text{dn}}$, where τ_{dn} is the down-leg travel time. The transmission time at the tracking station is therefore given by $t - \tau_{\text{dn}} - \tau_{\text{up}}$, where τ_{up} is the up-leg travel time.

Therefore, the determination of the range-rate comprises two iterative light time solutions for the up-leg and the down-leg, respectively. For the initialisation the travel time is not known and set to zero (Eq. 5.1) (Montenbruck and Gill, 2001).

$$\begin{aligned}\tilde{\tau}_{\text{dn}} &= 1/c \cdot |\mathbf{r}_3(t_3) - \mathbf{r}_2(t_3)| \\ t_2 &= t_1 - \tilde{\tau}_{\text{dn}} = t_1 - 1/c \cdot |\mathbf{r}_3(t_3) - \mathbf{r}_2(t_3)|\end{aligned}\tag{5.1}$$

After the first iteration the down-leg travel time is available and the solution is improved till a certain threshold is reached (Eq. 5.2).

$$t_2 = t_1 - \tau_{\text{dn}} = t_1 - 1/c \cdot |\mathbf{r}_3(t_3) - \mathbf{r}_2(t_3 - \tau_{\text{dn}})|\tag{5.2}$$

The same procedure is than repeated for the up-link travel time. Since the **GRAIL** mission orbits the Moon, the light time solution has to be computed in the barycentric reference frame. Hence, the relativistic light time delay has to be considered.

5.1.2. Light Time Equation

The relativistic light time delay, due to each body of the solar-system, accounts for the increase in the light time. The light time equation in the solar-system barycentric frame is given by

$$\begin{aligned}t_2 - t_1 &= \frac{r_{12}}{c} + \frac{(1 + \gamma)GM_{\text{S}}}{c^3} \cdot \ln \left[\frac{r_1^{\text{S}} + r_2^{\text{S}} + r_{12}^{\text{S}}}{r_1^{\text{S}} + r_2^{\text{S}} - r_{12}^{\text{S}}} \right] \\ &+ \sum_{\text{B}} \frac{(1 + \gamma)GM_{\text{B}}}{c^3} \cdot \ln \left[\frac{r_1^{\text{B}} + r_2^{\text{B}} + r_{12}^{\text{B}}}{r_1^{\text{B}} + r_2^{\text{B}} - r_{12}^{\text{B}}} \right],\end{aligned}\tag{5.3}$$

where GM_{S} is the gravitational constant of the Sun and GM_{B} is the gravitational constant of a planetary body. For general relativity $\gamma \approx 1$ holds true. The time t_1 refers to the transmission time at a tracking station on Earth, t_2 refers to the reflection time at the spacecraft. The reception time at a tracking station on Earth is denoted by t_3 . Hence, Eq. 5.3 is the up-leg light time equation. The corresponding down-leg light time equation is obtained by replacing the indices 1 with 2 and 2 with 3 (Moyer, 2000).

The first term on the right side of Eq. 5.3 is the time for light to travel from the tracking station to the satellite along a straight-line path at the speed of light c . This is the Newtonian light time. The second and third term of the equation accounts for the reduction of the light velocity and the bending of the light path. The term is evaluated for the Sun and selected celestial bodies of the solar system.

5.1.3. Algorithm

The starting point for the calculation of the light time solution is the reception time t_3 . In the case of a satellite tracked by a DSN tracking station on Earth, the time t_3 is at the station location. The spacecraft light time solution for the down-leg is obtained by performing the following steps:

1. Transformation of the reception time t_3 from UTC to TAI.

$$t_3(\text{UTC}) \rightarrow t_3(\text{TAI}) \quad (5.4)$$

2. Transformation of the reception time t_3 from TAI to ET according to Eq. 2.6. From now on all mentioned times are in ET. Depending on the used coordinate frame the TDT is used for geocentric frames, while the TDB is used for coordinates in the barycentric frame.

$$t_3(\text{TAI}) \rightarrow t_3(\text{ET}) \quad (5.5)$$

3. Determination of the space-fixed positions in the solar-system barycentric frame for the planetary bodies at time t_3 . Calculation of the geocentric space-fixed positions for the tracking station at time t_3 .

$$\mathbf{r}_S^C(t_3), \mathbf{r}_J^C(t_3), \mathbf{r}_{\text{Sa}}^C(t_3), \mathbf{r}_E^C(t_3), \mathbf{r}_M^C(t_3), \mathbf{r}_3^G(t_3) \quad (5.6)$$

C denotes the solar-system barycentric frame and G the geocentric frame. S stands for the Sun, J for Jupiter, Sa for Saturn, E for the Earth and M for the Moon. If the celestial bodies in general are meant, a B is used. As already mentioned, the tracking station at the time t_3 is labelled with the subscript 3.

4. Addition of the geocentric space fixed position of the tracking station on Earth to the solar-system barycentric position vectors of the Earth to get the solar-system barycentric position.

$$\mathbf{r}_3^C(t_3) = \mathbf{r}_3^G(t_3) + \mathbf{r}_E^C(t_3) \quad (5.7)$$

Chapter 5. Methodology

5. For each planetary body, for which the relativistic light time delay is calculated, calculation of the vector and scalar distance from the body to the tracking station at the reception time t_3 .

$$\begin{aligned}\mathbf{r}_3^B(t_3) &= \mathbf{r}_3^C(t_3) - \mathbf{r}_B^C(t_3) \\ r_3^B(t_3) &= |\mathbf{r}_3^B(t_3)|\end{aligned}\quad (5.8)$$

6. For the initialisation of the iteration zero is used for the predicted light time. To speed up the processing an approximation can be computed and used as initial value. For all following solutions the light time can be calculated from Eq. 5.9.

$$\Delta t_{23} = t_3 - t_2 = \frac{|\mathbf{r}_3 - \mathbf{r}_{20} - \dot{\mathbf{r}}_{20} \Delta t_3|}{c}\quad (5.9)$$

Subtraction of the predicted light time from the reception time t_3 to get the first estimation of the transmission time t_2 at the spacecraft.

$$t_2 = t_3 - \Delta t_{23}\quad (5.10)$$

7. Interpolation of the celestial ephemeris for the estimated transmission time t_2 at the spacecraft.

$$\mathbf{r}_S^C(t_2), \mathbf{r}_J^C(t_2), \mathbf{r}_{Sa}^C(t_2), \mathbf{r}_E^C(t_2), \mathbf{r}_M^C(t_2), \mathbf{r}_3^G(t_2)\quad (5.11)$$

8. Interpolation of the spacecraft ephemeris for the estimated transmission time t_2 . Addition of the solar-system barycentric position of the central body to get the spacecraft position in the solar-system barycentric frame.

$$\mathbf{r}_2^C(t_2) = \mathbf{r}_2^M(t_2) + \mathbf{r}_M^C(t_2)\quad (5.12)$$

9. Calculation of the vector and scalar distance from each body in the light time delay to the spacecraft at the transmission time t_2 .

$$\begin{aligned}\mathbf{r}_2^B(t_2) &= \mathbf{r}_2^C(t_2) - \mathbf{r}_B^C(t_2) \\ r_2^B(t_2) &= |\mathbf{r}_2^B(t_2)|\end{aligned}\quad (5.13)$$

10. Determination of vectors, scalars and the relativistic light time along the down-leg from the spacecraft to the tracking station on Earth derived from Eq. 5.3 in Eq. 5.15.

$$\begin{aligned}\mathbf{r}_{23} &= \mathbf{r}_3^C(t_3) - \mathbf{r}_2^C(t_2) \\ r_{23} &= |\mathbf{r}_{23}| \\ \dot{r}_{23} &= \frac{\mathbf{r}_{23}}{r_{23}} \cdot \dot{\mathbf{r}}_{23} \\ \dot{\rho}_{23} &= \frac{\mathbf{r}_{23}}{r_{23}} \cdot \dot{\mathbf{r}}_2^C(t_2)\end{aligned}\quad (5.14)$$

$$\begin{aligned}
 RLT_{23} = & \frac{(1 + \gamma)GM_S}{c^3} \cdot \ln \left[\frac{r_2^S + r_3^S + r_{23}^S}{r_2^S + r_3^S - r_{23}^S} \right] \\
 & + \sum_B \frac{(1 + \gamma)GM_B}{c^3} \cdot \ln \left[\frac{r_2^B + r_3^B + r_{23}^B}{r_2^B + r_3^B - r_{23}^B} \right]
 \end{aligned} \tag{5.15}$$

These quantities are computed from the solar-system barycentric vectors calculated until now in the process.

11. With t_3 and the current estimation for the transmission time t_2 at the spacecraft, the linear differential correction Δt_2 can be calculated. If Δt_2 is added to the current t_2 , the next estimation for the transmission time t_2 is given.

$$\begin{aligned}
 \Delta t_2 = & \frac{t_3 - t_2 - \frac{r_{23}}{c} - RLT_{23}}{1 - \frac{\dot{r}_{23}}{c}} \\
 t_2 = & t_2 + \Delta t_2
 \end{aligned} \tag{5.16}$$

12. If the absolute value of Δt_2 is less than 10^{-10} seconds, the algorithm proceeds with step 13. Otherwise the next step is 6 again for the next iteration. If a feasible solution is not obtained after five iterations the execution is halted.
13. Re-computation of all coordinates with the last and final estimate $t_2 + \Delta t_2$ for the reflection time.

For the algorithm of the up-leg to determine the transmission time t_1 , the algorithm of the down-leg with a few adjustments can be used. First the indexes 3 and 2 have to be replaced by 1 and 2. Also the initialisation process is not needed. Hence, the determination can start at step 6.

5.2. Range Difference

The range-rate \dot{r} is usually formulated as the difference of two ranges divided by the counting interval dt . Meaning that the range between the tracking station on Earth and the satellite at the beginning (t_{begin}) and the end (t_{end}) of the counting interval are differenced (Eq. 5.18). Therefore new time stamps are defined. The available time from the ODF is the receiving time t_3 (hereinafter referred to as $t_{\text{end},3}$) at the end of the counting interval. The receiving time at the beginning of the count interval is

$$t_{\text{begin},3} = t_{\text{end},3} - dt. \tag{5.17}$$

Consequently the transmitting and reflection times at the begin of the count interval are $t_{\text{begin},1}$ and $t_{\text{begin},2}$, the times at the end of the count interval are $t_{\text{end},1}$ and $t_{\text{end},2}$. These times were already determined by the light time solution.

$$\dot{r} = \frac{r(t_{\text{end},1}, t_{\text{end},2}) - r(t_{\text{begin},1}, t_{\text{begin},2})}{dt} \quad (5.18)$$

Eq. 5.18 is the range-rate for the up-leg, i.e. 1-way Doppler data. Both ranges r are determined between the tracking station at the transmitting times t_1 and the satellite at the reflection time t_2 .

In the case at hand 2-way Doppler data is used. Hence the determination is split in two. That means that the range difference is once calculated for the up-leg solution and additionally for the down-leg solution (Eq. 5.19).

$$\begin{aligned} \Delta r_{\text{up}} &= r_{\text{up}}(t_{\text{end},1}, t_{\text{end},2}) - r_{\text{up}}(t_{\text{begin},1}, t_{\text{begin},2}) \\ \Delta r_{\text{dn}} &= r_{\text{dn}}(t_{\text{end},2}, t_{\text{end},3}) - r_{\text{dn}}(t_{\text{begin},2}, t_{\text{begin},3}) \end{aligned} \quad (5.19)$$

In the case of 2-way Doppler data both ranges differences are added up to generate the range-rate (Eq. 5.20).

$$\begin{aligned} \dot{r}_{1\text{-way}} &= \frac{\Delta r_{\text{up}}}{dt} \\ \dot{r}_{2\text{-way}} &= \frac{\Delta r_{\text{up}} + \Delta r_{\text{dn}}}{dt} \end{aligned} \quad (5.20)$$

The scheme in Fig. 5.3 shows the determination for 1-way Doppler data. The ranges are determined at the begin and the end of the counting interval and afterwards differenced. The division by the counting interval is postponed at this point, due to the introduction of the observation corrections in the next section.

For the following algorithm the times at the beginning of the count interval are denoted as time 1, while time 2 stands for the times at the end of the counting interval (Fig. 5.3).

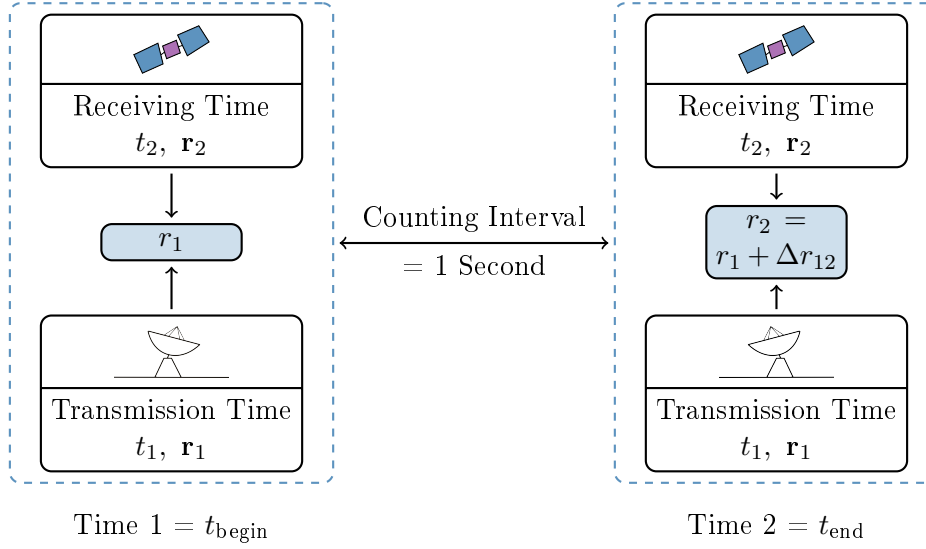


Figure 5.3.: Schema for 1-way Doppler range-rate determination

5.2.1. Algorithm

For an Earth orbiting satellite this differencing does not provide any numerical problems. Due to the size of ranges for interplanetary satellites, the following technique is necessary to avoid numerical errors. Therefore the range difference is expanded into a multidimensional Taylor series according to the [GEODYN](#) system description ([McCarthy et al., 1993](#)).

The distance vector between the tracking station and the satellite for time 1 is

$$\mathbf{r}_1 = (\mathbf{r}_E^C + \mathbf{r}_{\text{Stat}}^E) - (\mathbf{r}_P^C + \mathbf{r}_{\text{Sat}}^P), \quad (5.21)$$

where \mathbf{r}_E^C is the solar-system barycentric Earth position and \mathbf{r}_P^C is the solar-system barycentric central body position e.g. the position of the Moon. The planet-centred satellite position is denoted as $\mathbf{r}_{\text{Sat}}^P$, and $\mathbf{r}_{\text{Stat}}^E$ is the Earth-centred station coordinates.

For the distance vector at time 2 the relative change vectors are added

$$\mathbf{r}_2 = (\mathbf{r}_E^C + \Delta\mathbf{r}_E^C + \mathbf{r}_{\text{Stat}}^E + \Delta\mathbf{r}_{\text{Stat}}^E) - (\mathbf{r}_P^C + \Delta\mathbf{r}_P^C + \mathbf{r}_{\text{Sat}}^P + \Delta\mathbf{r}_{\text{Sat}}^P). \quad (5.22)$$

For simplification the following substitutions in [5.23](#) and [5.24](#) are used in the subsequent formulas:

$$\begin{aligned} r_x &= x_E^C + x_{\text{Stat}}^E - x_P^C - x_{\text{Sat}}^P \\ r_y &= y_E^C + y_{\text{Stat}}^E - y_P^C - y_{\text{Sat}}^P, \\ r_z &= z_E^C + z_{\text{Stat}}^E - z_P^C - z_{\text{Sat}}^P \end{aligned} \quad (5.23)$$

Chapter 5. Methodology

$$\begin{aligned}
 \Delta r_x &= \Delta x_E^C + \Delta x_{\text{Stat}}^E - \Delta x_P^C - \Delta x_{\text{Sat}}^P \\
 \Delta r_y &= \Delta y_E^C + \Delta y_{\text{Stat}}^E - \Delta y_P^C - \Delta y_{\text{Sat}}^P \\
 \Delta r_z &= \Delta z_E^C + \Delta z_{\text{Stat}}^E - \Delta z_P^C - \Delta z_{\text{Sat}}^P
 \end{aligned} \quad . \quad (5.24)$$

With 5.23 and 5.24, the range at time 1 is

$$r_1 = \sqrt{r_x^2 + r_y^2 + r_z^2}, \quad (5.25)$$

and the range at time 2 is

$$r_2 = \sqrt{(r_x + \Delta r_x)^2 + (r_y + \Delta r_y)^2 + (r_z + \Delta r_z)^2}. \quad (5.26)$$

The range at time 2 can be expressed in terms of the range at time 1 and becomes a function of Δr_x , Δr_y and Δr_z (Eq. 5.27).

$$\begin{aligned}
 r_2 &= \sqrt{r_1^2 + 2r_x\Delta r_x + 2r_y\Delta r_y + 2r_z\Delta r_z + \Delta r_x^2 + \Delta r_y^2 + \Delta r_z^2} \\
 &= f(\Delta r_x, \Delta r_y, \Delta r_z)
 \end{aligned} \quad (5.27)$$

After the subtraction of the ranges at time 1 and 2, the zero order term of this expression is eliminated and the range difference becomes a Taylor series of directional derivatives

$$\Delta r = r_2 - r_1 = f_\alpha(0, 0, 0) \times |\Delta \mathbf{r}| + f_{\alpha\alpha}(0, 0, 0) \times |\Delta \mathbf{r}|^2 + f_{\alpha\alpha\alpha}(0, 0, 0) \times |\Delta \mathbf{r}|^3 \quad (5.28)$$

with the change vector

$$\Delta \mathbf{r} = \Delta r_x \mathbf{e}_x + \Delta r_y \mathbf{e}_y + \Delta r_z \mathbf{e}_z \quad (5.29)$$

and the unit change vector

$$\boldsymbol{\alpha} = \frac{\Delta r_x}{|\Delta \mathbf{r}|} \mathbf{e}_x + \frac{\Delta r_y}{|\Delta \mathbf{r}|} \mathbf{e}_y + \frac{\Delta r_z}{|\Delta \mathbf{r}|} \mathbf{e}_z. \quad (5.30)$$

If

$$a = \frac{\Delta r_x}{|\Delta \mathbf{r}|}, \quad b = \frac{\Delta r_y}{|\Delta \mathbf{r}|}, \quad c = \frac{\Delta r_z}{|\Delta \mathbf{r}|} \quad (5.31)$$

then the derivatives are

$$\begin{aligned} f_\alpha &= \frac{a\Delta r_x + b\Delta r_y + c\Delta r_z}{r_1} \\ f_{\alpha\alpha} &= \frac{r_1 + \frac{1}{r_1}(a\Delta r_x + b\Delta r_y + c\Delta r_z)^2}{r_1^2} \\ f_{\alpha\alpha\alpha} &= \frac{r_1(a\Delta r_x + b\Delta r_y + c\Delta r_z)(-1 - 2(a + b + c)) + \frac{3}{r_1}(a\Delta r_x + b\Delta r_y + c\Delta r_z)^3}{r_1^2}. \end{aligned} \quad (5.32)$$

5.3. Observation Corrections

During the travel of a signal to a satellite and back again various influences act on it and therefore have an influence on the measured quantities. The main impacts are the troposphere and relativistic effects.

5.3.1. Tropospheric Correction

The propagation of the signal is mainly affected by the temperature, the atmospheric pressure and the partial pressure of water vapour. The contribution of the dry air is dominant in the correction and can be modelled reasonably well. The wet component can be modelled only poorly due to its high variability. The correction is therefore split into a dry and wet correction and is expressed as a path delay.

The Hopfield model uses the surface temperature T in degrees Kelvin (K), the surface pressure P in millibars (mb) and the partial water vapour pressure e in millibars (mb) as meteorological input parameters (Hopfield, 1971). The model is modified to use the Saastamoinen zenith range correction to determine the height of the troposphere appropriate for the wet and dry components (Saastamoinen, 1973).

With the parameter for the dry component N_1 (deviation from unity of the surface index of refraction, Eq. 5.33) and the parameter for the wet component N_2 (Eq. 5.34), the dry troposphere height in meters (m) is determined from Eq. 5.35 and the wet troposphere height in meters (m) is given by Eq. 5.36 (Montenbruck and Gill, 2001).

$$N_1 = 77.624 \cdot \frac{P}{T} \quad (5.33)$$

$$N_2 = 371900 \cdot \frac{e}{T^2} - 12.92 \frac{e}{T} \quad (5.34)$$

$$h_{\text{dry}} = h_1 = \frac{5.0 \cdot 0.002277}{N_1 \cdot 10^{-6}} P \quad (5.35)$$

$$h_{\text{wet}} = h_2 = \frac{5.0 \cdot 0.002277}{N_2 \cdot 10^{-6}} \left[\frac{1255}{T} + 0.05 \right] e \quad (5.36)$$

The tropospheric range correction for the Hopfield model is given by a ninth-order polynomial

$$\Delta r_{\text{tropo}} = C \left[\frac{N_1}{10^6} \sum_{i=1}^9 \frac{c_{i1} r_1^i}{i} + \frac{N_2}{10^6} \sum_{i=1}^9 \frac{c_{i2} r_2^i}{i} \right], \quad (5.37)$$

with the constant

$$C = \left[\frac{170.2649}{173.3 - \frac{1}{\lambda^2}} \right] \left[\frac{78.8828}{77.624} \right] \left[\frac{173.3 + \frac{1}{\lambda^2}}{173.3 - \frac{1}{\lambda^2}} \right] \approx 1 \quad (5.38)$$

for radio frequencies. The wavelength of transmission is denoted as λ and is required in microns. The distance to the top of the dry ($j = 1$) and wet ($j = 2$) troposphere is

$$r_j = \sqrt{(\alpha_e + h_j)^2 - (\alpha_e \cos(E))^2} - \alpha_e \sin(E) \quad (5.39)$$

where α_e denotes the semi-major axis of the Earth and E denotes the elevation angle. The polynomial coefficients are according to [McCarthy et al. \(1993\)](#) in the [GEODYN](#) system description and are defined as follows

$$\begin{aligned} c_{1j} &= 1 \\ c_{2j} &= 4a_j \\ c_{3j} &= 6a_j^2 + 4b_j \\ c_{4j} &= 4a_j(a_j^2 + 3b_j) \\ c_{5j} &= a_j^4 + 12a_j^2 b_j \\ c_{6j} &= 4a_j b_j (a_j^2 + 3b_j) \\ c_{7j} &= b_j^2 (6a_j^2 + 4b_j) \\ c_{8j} &= 4a_j b_j^3 \\ c_{9j} &= b_j^4 \end{aligned} \quad (5.40)$$

with the substitutions

$$\begin{aligned} a_j &= \frac{-\sin(E)}{h_j} \\ b_j &= \frac{-\cos(E)^2}{2h_j\alpha_e}. \end{aligned} \tag{5.41}$$

5.3.2. Relativistic Correction

The relativistic correction in Eq. 5.42 is a combination of the general and special relativity. These corrections are computed in the light time solution (Eq. 2.7, 5.15).

$$\Delta r_{\text{rel}} = \frac{RLT + \Delta ET}{c} \tag{5.42}$$

5.4. Ramped Frequency

As a last step the computed observable, which is now corrected but still a geometric quantity in meters, becomes a frequency. The used frequency consists of two parts: a constant base frequency and a ramped frequency part.

According to McCarthy et al. (1993) the constant frequency is determined by

$$f_{\text{const}} = \left[dt - \frac{\Delta r}{c} \right] f_b \cdot sf_2 - dt \cdot bias, \tag{5.43}$$

where dt is the counting interval, Δr is the range difference, f_b is the ramp base frequency and sf_2 denotes the turn-around ratio. The bias term is taken from the G2B file (Item 9 in Table A.4) and is the reference frequency scaled by the turn-around ratio.

For the ramped term additional time tags are defined. The start time of the ramp interval is denoted as t_s . For the case that transmission times t_1 from the beginning and the end of the count interval are in the same ramp interval, the mid point of the interval is denoted as t_0 . For the time t_0 the current ramp frequency f_0 is determined with

$$f_0(t_0) = f(t_s) + \dot{f}(t_s - t_0), \tag{5.44}$$

where $f(t_s)$ is the ramp start frequency of the current ramp interval and $\dot{f}(t_s - t_0)$ is the ramp rate of the current ramp interval at the time t_0 . In the case that the transmission

times are in different ramp intervals the determination is split in two. Two times at the midpoint between the transmission times and the ramp start time are defined and used as times t_0 . The frequencies are afterwards multiplied with the time span the ramp information is used and added.

The interval width is

$$w = t_e - t_s, \quad (5.45)$$

where t_e denotes the end time tag of the ramp interval. Together with the turn-around ratio it forms the ramped term (Eq. 5.46).

$$f_{\text{ramp}} = w \cdot f_0 \cdot s f_2 \quad (5.46)$$

The sum of the two frequency terms divided by the counting interval dt results in the desired calculated observable (O) in Hertz (Eq. 5.47).

$$O = \frac{f_{\text{const}} + f_{\text{ramp}}}{dt} \quad (5.47)$$

5.5. Overview

As Fig. 5.4 displays, the process of the observable computation starts with the light time solution. The algorithms for the down-leg and up-leg have to be performed twice. Once for the receiving time at the beginning of the counting interval and also for receiving time at the end of the counting interval. Therefore in the end there is for every observation a pair of receiving, reflection and transmission times.

The range difference Δr is determined from the computed times of the light time solution (Eq. 5.48, Fig. 5.4). Before the range differences are converted to a range-rate by the division with the counting interval dt , the observation corrections have to be applied. The corrections have an influence on the range between the tracking station and the satellite. Therefore this range modification has to be applied before the transformation to a range-rate.

$$\Delta r = \Delta r_{\text{up}} + \Delta r_{\text{down}} \quad (5.48)$$

The observation corrections Δr_{corr} have to be computed also at both the end and the beginning of the counting interval for the up- and down-leg. The differentiation is the same as in the determination of the range difference (Eq. 5.49).

$$\Delta r_{\text{corr}} = \Delta r_{\text{up}} + \Delta r_{\text{down}} + \Delta r_{\text{corr,up}} + \Delta r_{\text{corr,down}} \quad (5.49)$$

After the application of the time dependent ramped frequency and the division by the counting interval the range-rate is calculated. For the further process of the orbit determination the difference between the observed (O) and the computed (C) observations i.e. the residuals

$$\varepsilon = O - C \quad (5.50)$$

have to determined. These residuals are introduced as reduced observations for the least squares adjustment of the orbit.

Since not the whole orbit determination was implemented, simplifications were necessary. The process begins after the orbit determination and therefore assumes that the orbit of the satellite is already calculated. Hence the predicted orbit was extracted from **GEODYN**. The coordinates of the planetary bodies were derived from **SPICE** kernels¹. Also the **DSN** tracking station coordinates were already corrected for tidal deformations when they were used.

¹http://naif.jpl.nasa.gov/pub/naif/toolkit_docs/C/index.html

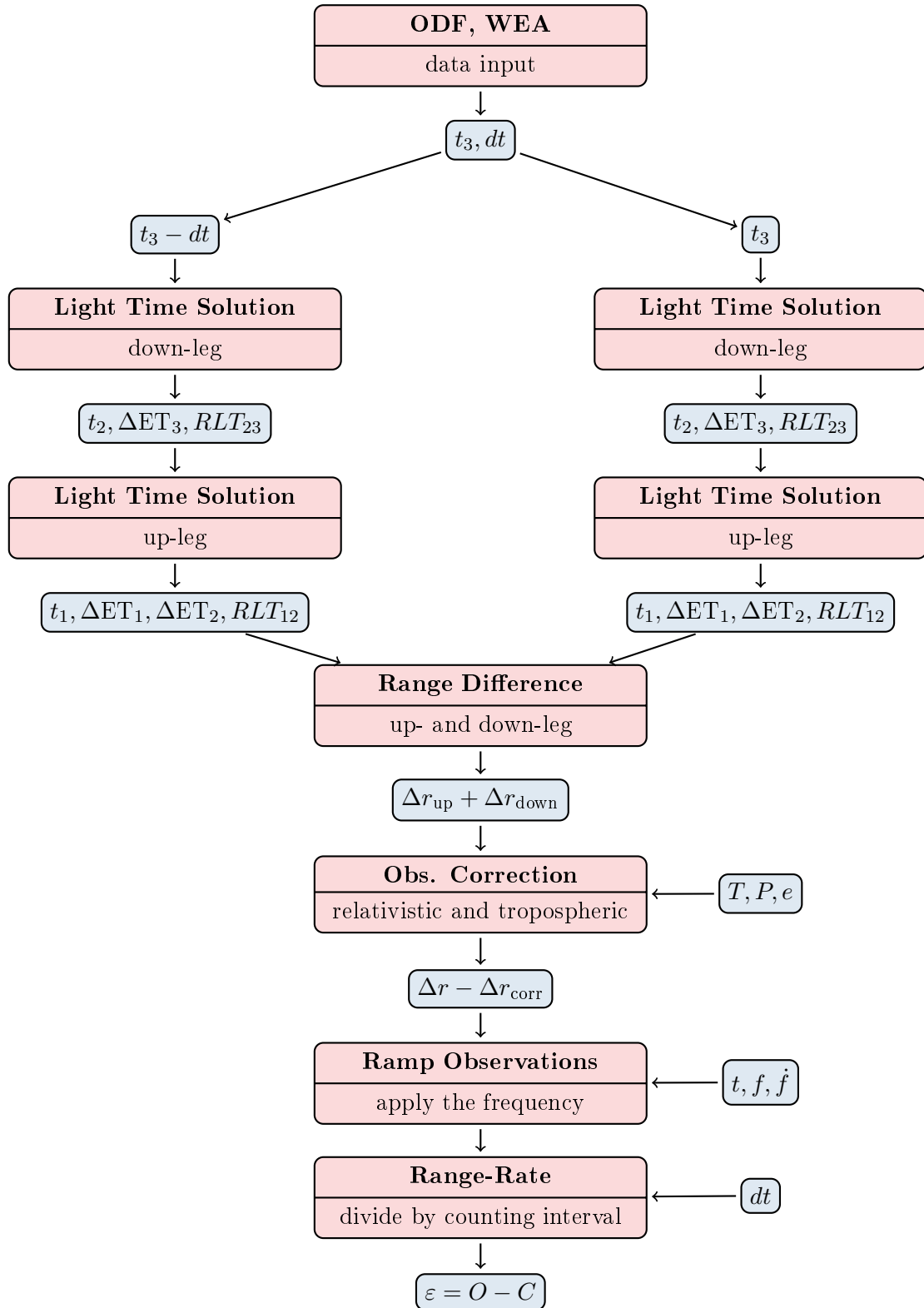


Figure 5.4.: Observation computation

Chapter 6.

Results

This chapter presents the result of the range-rate determination from the tracking data stored by the [DSN](#), including the comparison of the result to the reference solution. The results and the discussion are presented in a single interconnected chapter to emphasize the sequential research objectives.

6.1. Files Formats and Contents

The first question to be answered concerned the content of the stored tracking data of the [DSN](#) in the [ODF](#). With the help of a self written Fortran script it was possible to convert the binary file into an [ASCII](#) file. [Figure 6.1](#) shows the extracted 1-way and 2-way Doppler data in Hertz. The displayed data acts in accordance with the the physical principle of the Doppler effect. The frequency received on the ground is higher or lower than the transmitted frequency. The deviation depends on the location of the observer and whether the distance between the satellite and observer is decreasing or increasing. The same principle is illustrated in [Fig. 2.1](#). When the minimum distance between the satellite and the receiver is reached, the Doppler effect is zero. This behaviour can be perfectly seen in the 1-way Doppler data. In the 2-way Doppler data this characteristic is distorted due to the fact that the frequency is ramped.

[Figure 6.3](#) shows the ramped frequency. The similarity to the Doppler curve and therefore the observations is apparent. The ramp start frequencies of the ramp intervals are marked with crosses. The curves in the background are the change rates determined at each second. By computing the ramped frequency at each observation epoch, the visible curves can be determined. Meaning that each observation has its own specific station dependent ramped frequency.

Also a displacement of the data shown in [Fig. 6.1](#) can be detected. This leap in the data is due to a change of the reference frequency at the ground station ([Fig. 6.2](#)). The Doppler technique requires the use of a highly stable reference frequency on the

Chapter 6. Results

spacecraft. In the case of [GRAIL](#) this reference frequency is at the [DSN](#). The spacecraft derives the frequency from the uplink transmission frequency ([Noreen, 1995](#)). The leap in the data is complied by subtracting a bias term (Eq. 5.43) from the observable. The bias is the reference frequency, meaning the transmitted frequency at the tracking station, multiplied by the turn around ratio applied at the spacecraft.

According to [You et al. \(2012\)](#) the S-band 2-way Doppler data is the standard data type for the orbit determination solution. The X-band 1-way Doppler data is often available but is not included in the solution. Its limiting factor is a systematic response to the entry and exit to shadow ([Ryne et al., 2013](#)).

As stated by [Ryne et al. \(2013\)](#) the standard deviation of the in-flight 2-way Doppler data is between 0.002 Hz and 0.0008 Hz. The in-flight observed tracking data accuracy is much better than the pre-launch expectations (Table 6.1).

Data Type	Pre-Launch Assumption (1σ)	Observed (1σ)	Remark
2-Way Doppler	1 mm/s	0.10 - 0.15 mm/s	60 seconds sampling 1mm/s \approx 0.015 Hz

Table 6.1.: Pre-launch and observed tracking noise ([You et al., 2012](#))
[S-Band]

To determine an orbit, which is a necessary input for the computed observable, the software package [GEODYN II](#) was used. As input the information of the [ODF](#) file had to be converted into the [G2B](#) file format. The question arising was, whether the conversion from [ODF](#) to [G2B](#), changes the data. As detailed in [Appendix B](#) the observed tracking data is merely rearranged. [Figure 6.4](#) shows the difference of the measurements with the time tag of the [ODF](#). The [ODF](#) and [G2B](#) files converted to readable [ASCII](#) files have nine decimal places. The output file of the software package [GEODYN](#) displays also nine decimal places. That the observations are completely the same can be seen in the plots of [Fig. 6.4](#), where any difference of observations results in zero.

The most sensible part of the orbit determination, especially the computation of the observable, is the time. As mentioned in [Appendix A](#) the [G2B](#) time tag is at the end of the interval. Additionally delay corrections are added (Eq. 6.1). [Figure 6.5](#) shows the time difference of Modified Julian Date Seconds ([MJDS](#)) between the [ODF](#), [G2B](#) and [GEODYN](#) output. The first shown [DSN](#) station tracking the spacecraft has a station delay of 77 000 ns. The second tracking station has none and therefore the time difference is half the counting interval dt . The change between the stations can be seen in [Fig. 6.1](#). At the first switch, two stations observe parallel.

$$t_{\text{G2B}} = t_{\text{ODF}} + \frac{dt}{2} + \Delta t_{\text{delay}} \quad (6.1)$$

Chapter 6. Results

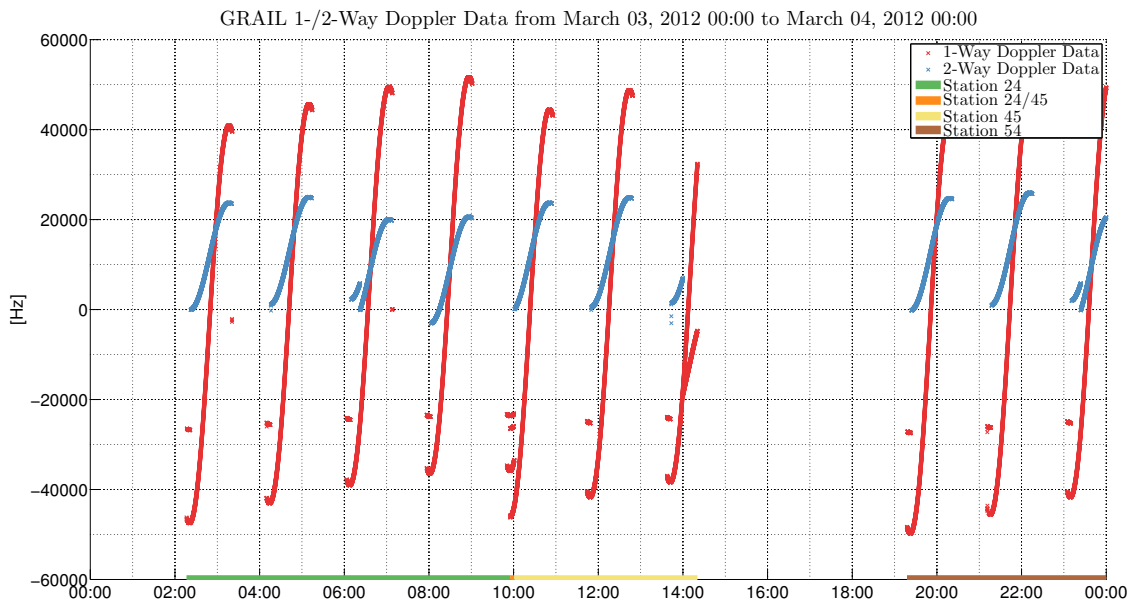


Figure 6.1.: 1- and 2-way Doppler data

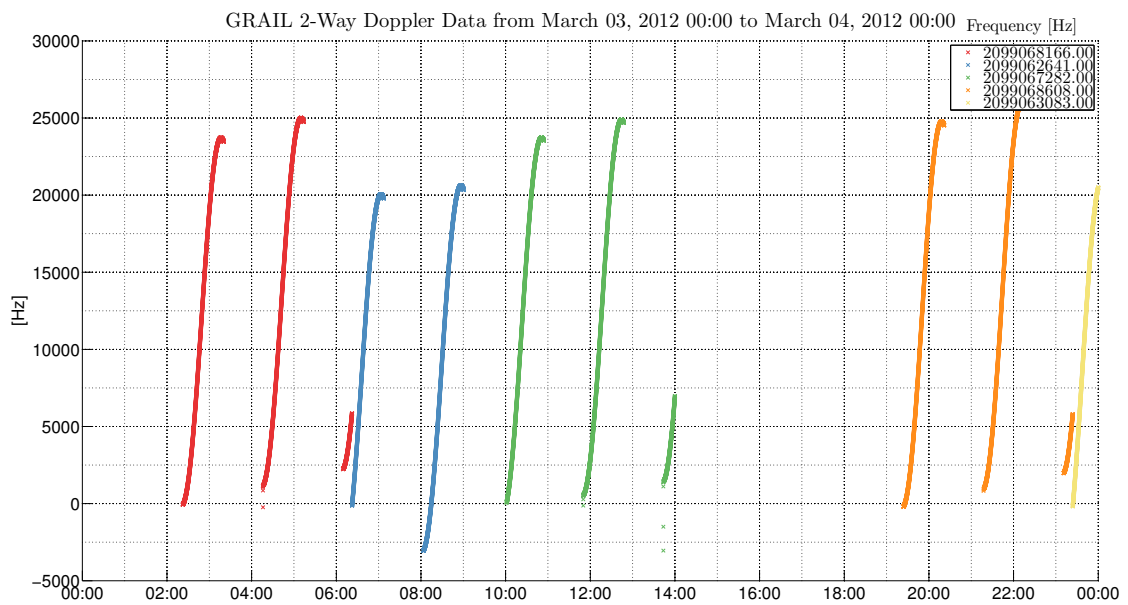


Figure 6.2.: Reference frequencies in the 2-way Doppler data

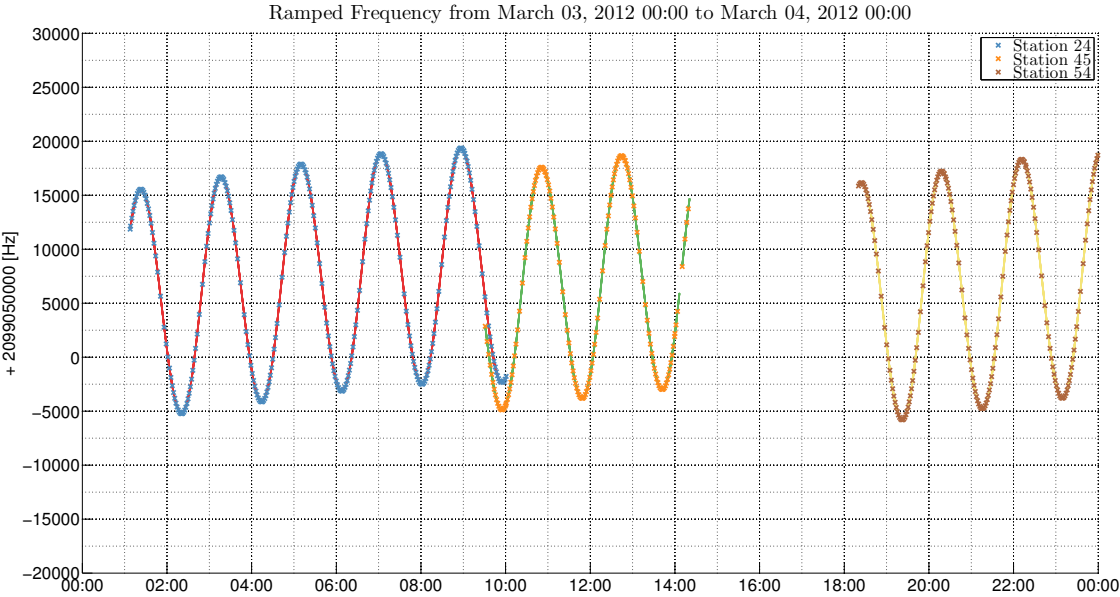


Figure 6.3.: Ramped frequency

Chapter 6. Results

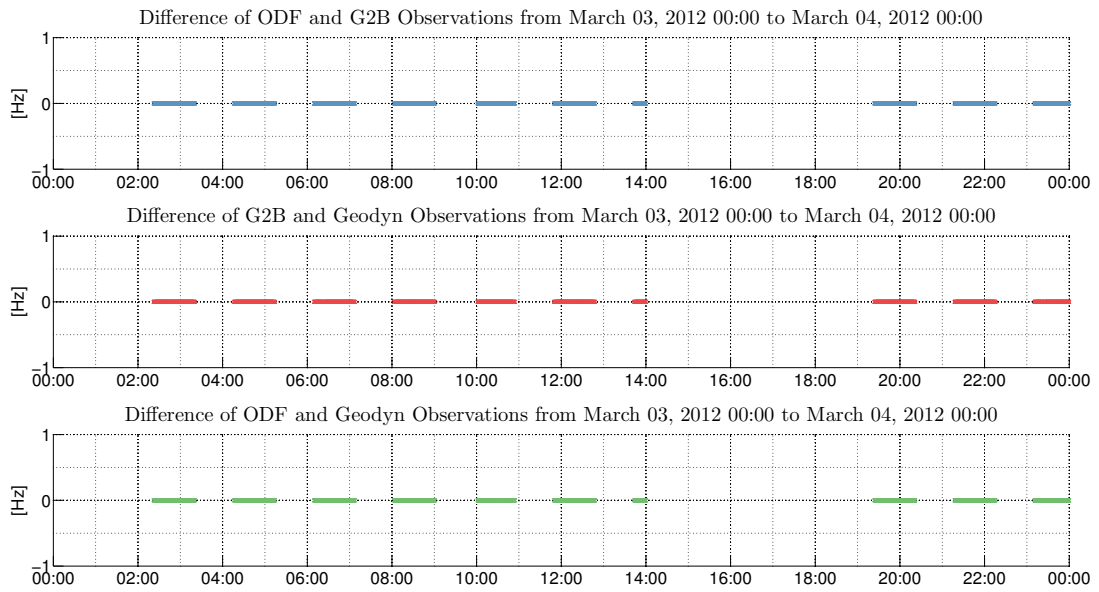


Figure 6.4.: Observation difference

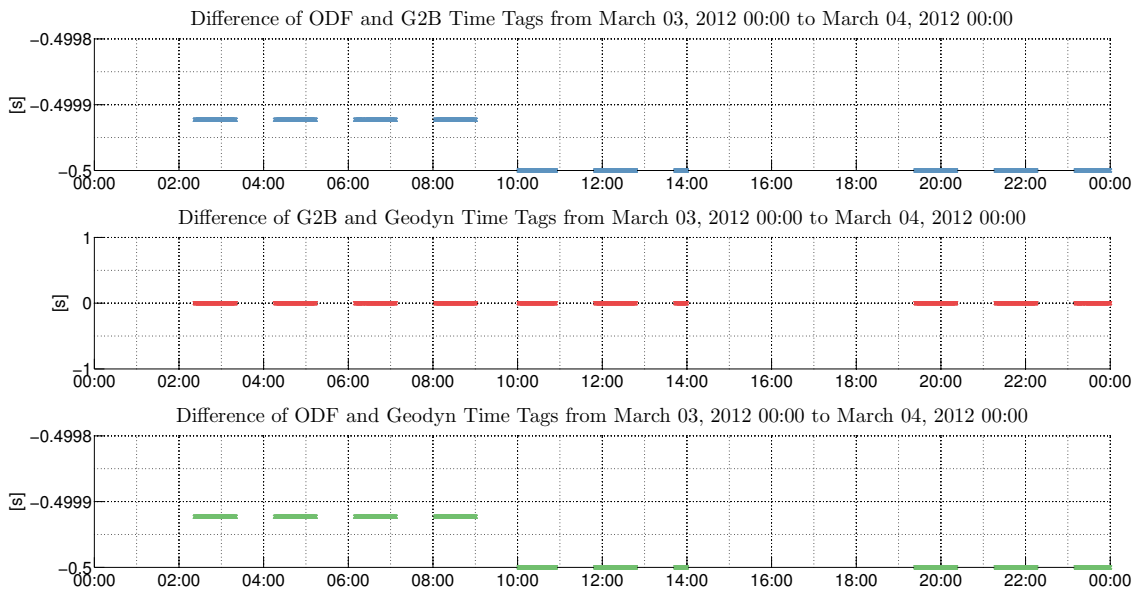


Figure 6.5.: Time difference

6.2. Orbit Determination

The orbit determination was calculated with the software package `GEODYN`. In a first step the input cards had to be adapted for the case at hand. As section 2.2 states different forces act upon the satellite. The more accurately these forces can be modelled, the better the orbit can be determined, starting from the initial state vector. Meaning that the selected parameters have an enormous influence on the output trajectory.

Figure 6.6 displays the result in the case of a simple forward integration. The determined orbit is subtracted from the official `JPL` orbit solution for `GRAIL`. According to [Konopliv et al. \(2013\)](#) the `JPL GRAIL` orbit was determined to an accuracy of 20 cm. In the beginning the model approximates the true reference orbit well. The further away, the worse gets the approximation. Meaning that model errors accumulate with the progression of time from the initial state vector. It can be seen clearly that the mismodeled or not modelled part is mostly pass dependent.

In contrast, Fig. 6.7 visualizes the result of the orbit determination with the observed data incorporated. Again, the difference between the determined orbit and the official product is shown. Here, the orbit is fitted to the observations. Since the initial state vector is extracted from an official `JPL` product, the a priori information is more accurate than the computed orbit. Due to the use of the observations, the orbit is improved. The X-coordinate shows very clearly the most deviation from the reference trajectory. To interpret the shown result better, the difference was transformed to the orbit system of `GRAIL`.

Figure 6.8 shows the difference between the `JPL` orbit and the determined orbit with `GEODYN` in the orbit system. In the radial and across-track direction only small variations occur. The main direction of movement is in the (quasi) along-track component. Due to the fact, that the non-conservative forces cannot be modelled properly, the quasi along-track component shows the most variation to the reference. In the case at hand the orbit determination was a secondary goal, and therefore the shown result was used for the further calculation.

Since the trajectory is fitted to the observations, the residuals, i.e. the observed observations minus the computed observations, are of interest. Figure 6.9 displays the residuals of the first and last iteration by `GEODYN`. The first iteration shows evidently how the prediction gets worse over time, while the last iteration displays residuals around zero. While some observations are evident outliers, Fig. 6.10 shows that also the eighth and ninth pass is affected. Due to mismodeling observations at the beginning and the end of the passes are detected as outliers.

Chapter 6. Results

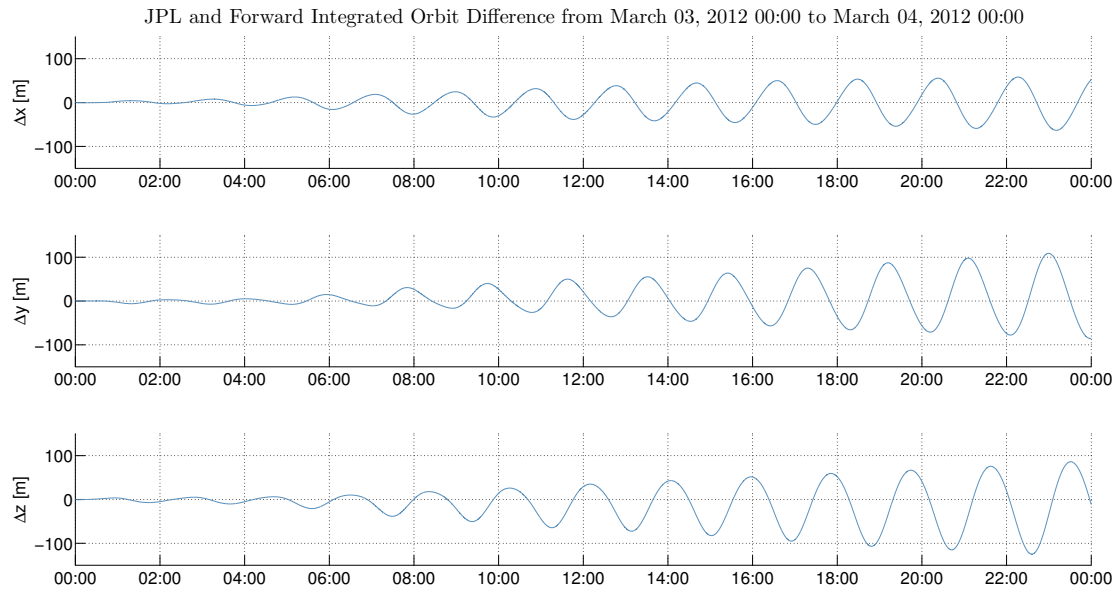


Figure 6.6.: Orbit comparison to JPL
[Forward integrated orbit, inertial system]

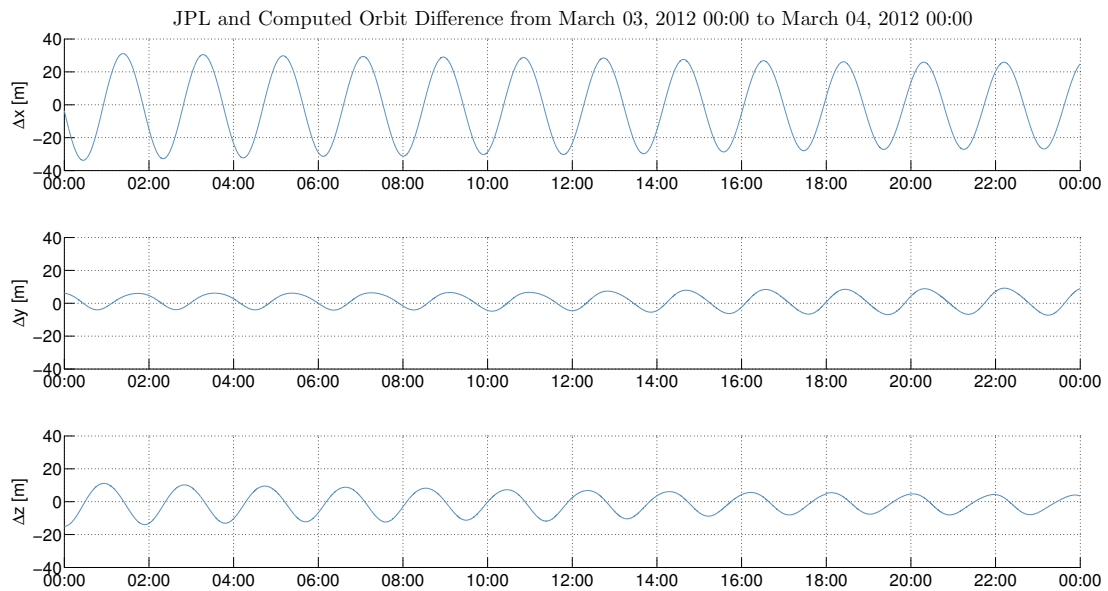


Figure 6.7.: Orbit comparison to JPL
[Orbit estimated according to observations, inertial system]

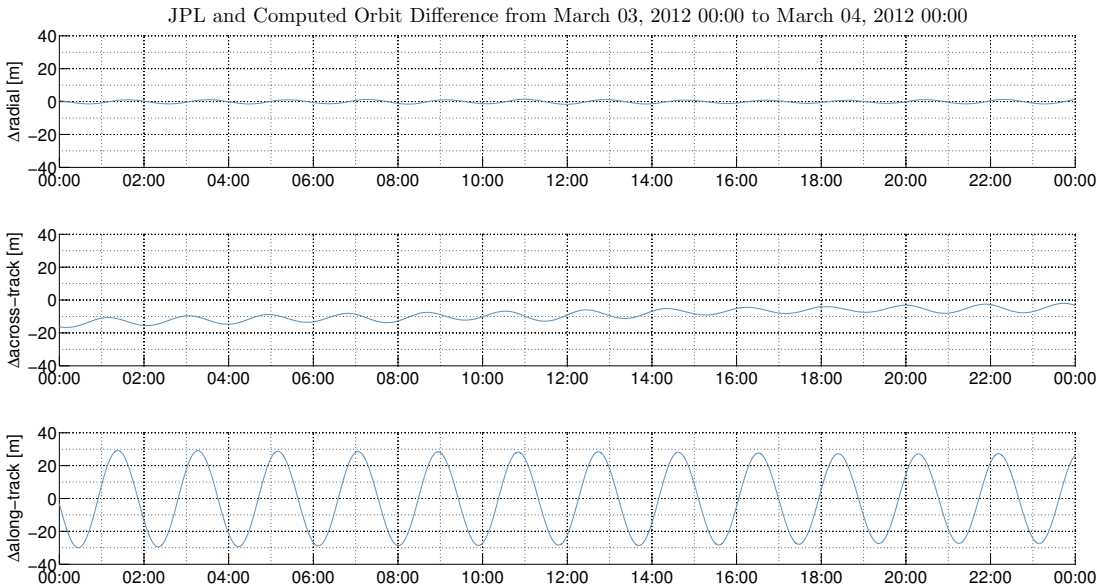


Figure 6.8.: Orbit comparison to JPL
[Orbit estimated according to observations, orbit system]

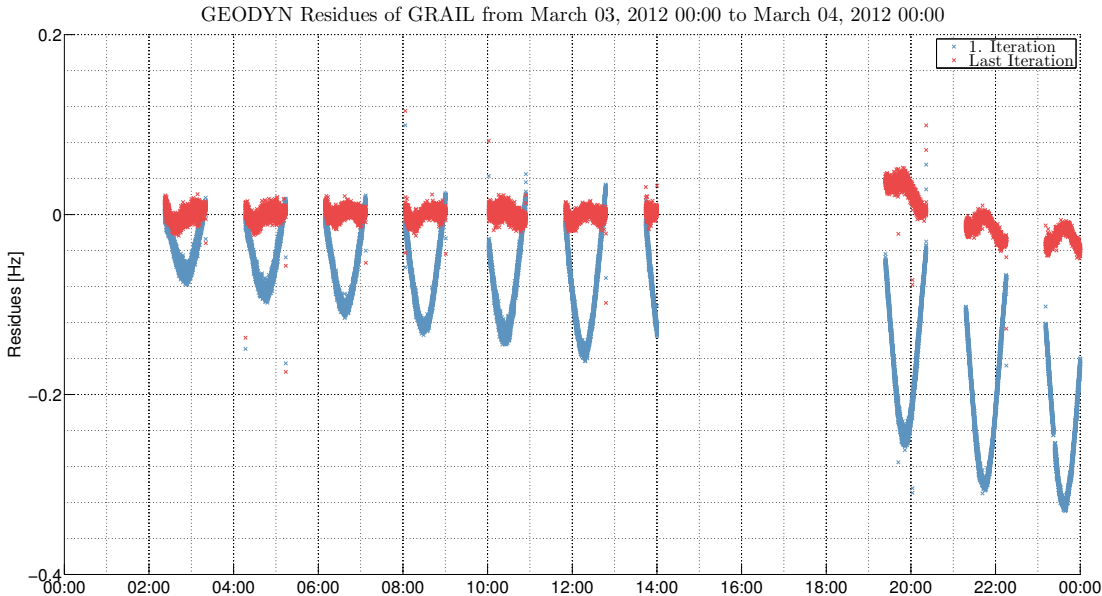


Figure 6.9.: 1st and last iteration residuals

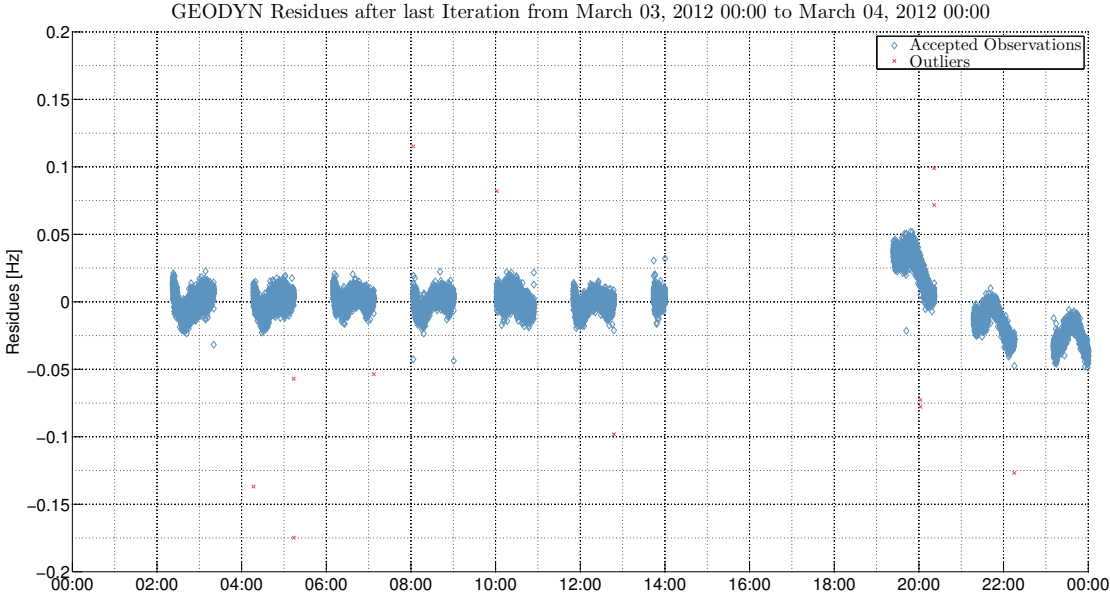


Figure 6.10.: Last iteration residuals with marked outliers

6.3. Range-Rate Determination

The computed observations were determined according to chapter 5. Figure 5.4 shows the computation till the residue of the observations. Originating from the receiving time at the end of the counting interval from the G2B file six times are computed in total. These times are then combined to determine the range difference as well as the observation corrections. By merging the geometric range differences information with the frequency and dividing it by the counting interval the computed observations in Hertz are calculated. In a last step the residuals, that is the difference between the observed and the computed observable, are computed. The aim is to reduce the residuals as best as possible and therefore adjusting the parameters and orbit to the observations.

It has to be noted that in the following figures and determinations the station dependent measurement corrections are not considered. Meaning that the residuals are determined and compared directly after their computation.

Figure 6.11 shows the residuals of GEODYN compared with the computed residuals in Hertz for the first iteration. The shape is due to the bad modelling, which influenced the predicted orbit. Then again, the orbit is an input to the range-rate determination. The determined range-rates and thereafter residuals fit well to the GEODYN residuals. Further details gives Fig. 6.12. Here the difference of the residuals is shown in velocity. The difference of the residuals is in the same magnitude as the observed standard deviation. It has to be remarked that in the case at hand a one second sampling was used. Meaning, that the reached accuracy is sufficient. Additionally a pass dependent linear behaviour is visible. This trend is due to a time dependent GEODYN center of integration velocity correction in the light time solution, which was not applied. This neglect causes a systematic deviation of the time in the magnitude of 10^{-7} seconds.

Figures 6.13 and 6.14 show the residuals and the difference of the residuals for the last iteration. Again the same behaviour is visible in the data. While the comparison shows a great similarity, the differences of the residuals shows the same trends as in the 1st iteration.

6.4. Numerical Considerations

One of the most challenging issues in the implementation was the time format and its conversion to different formats. Therefore this sections addresses firstly the different formats and secondly issues in the execution.

GEODYN refers its time tag to the GEODYN reference time. In a block of data, usually consisting of 40 observations, there is one block time tag w.r.t. the GEODYN reference time existing. It is given in UTC integer seconds since the reference time. Additionally,

Chapter 6. Results

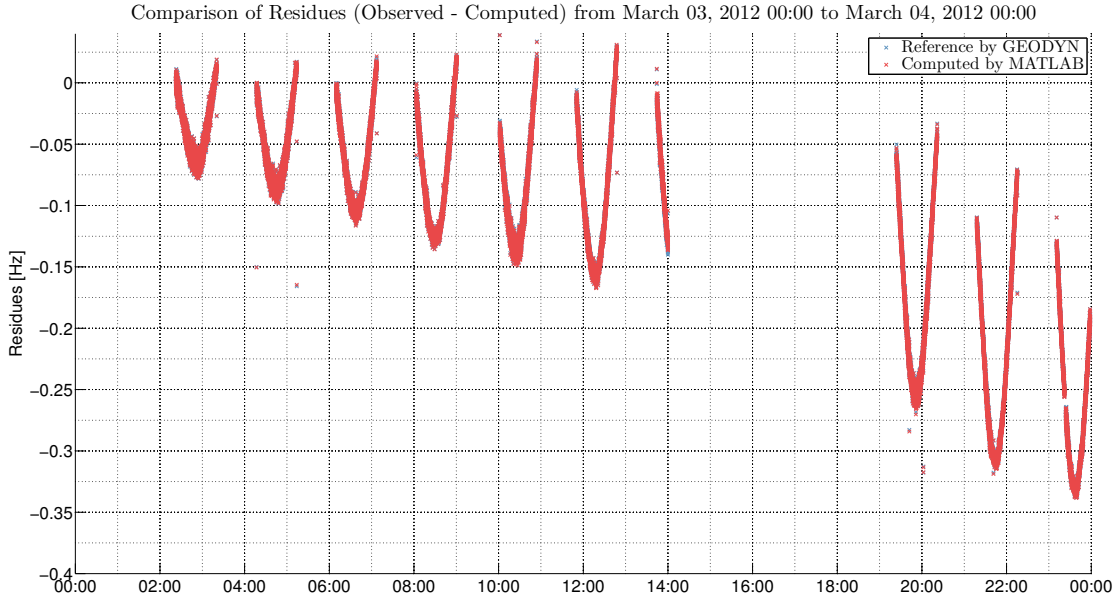


Figure 6.11.: Computed observable compared to GEODYN solution [1st iteration]

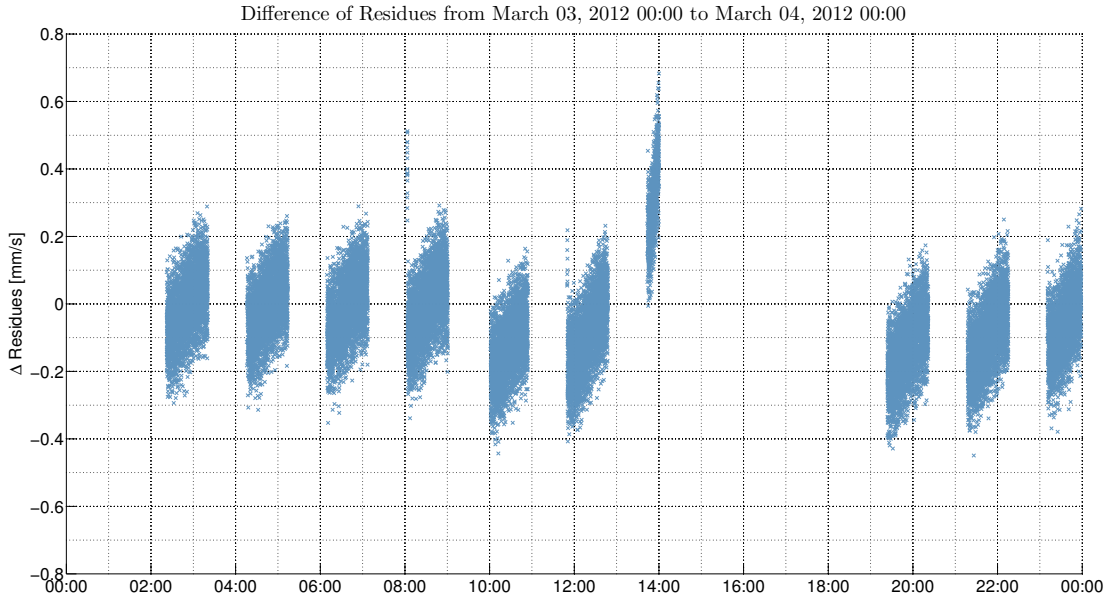


Figure 6.12.: Difference of computed observable with GEODYN solution [1st iteration]

Chapter 6. Results

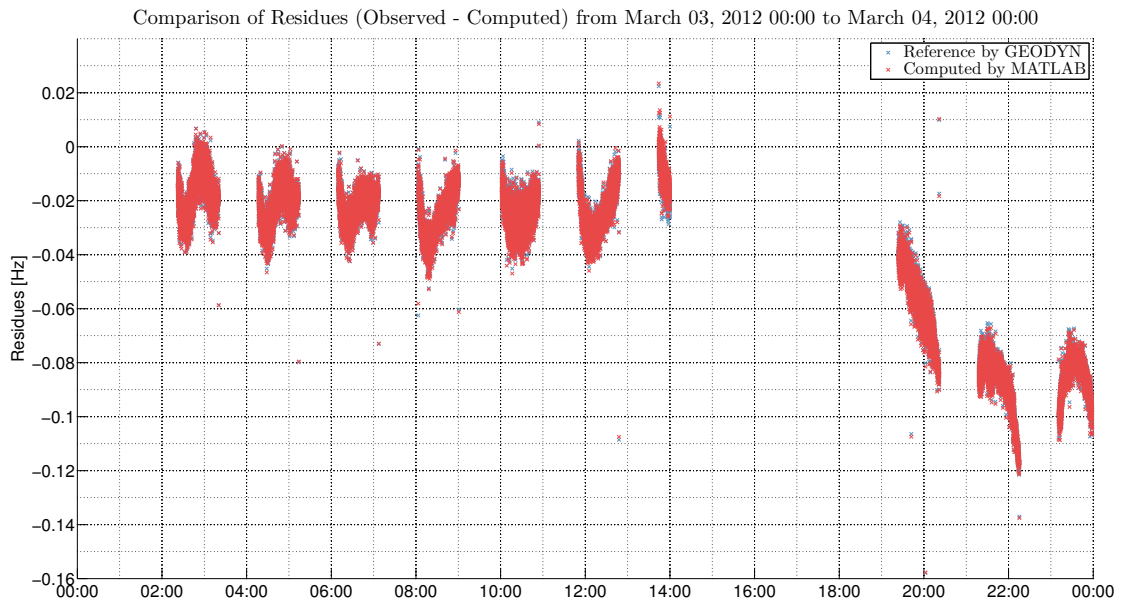


Figure 6.13.: Computed observable compared to GEODYN solution
[Last iteration]

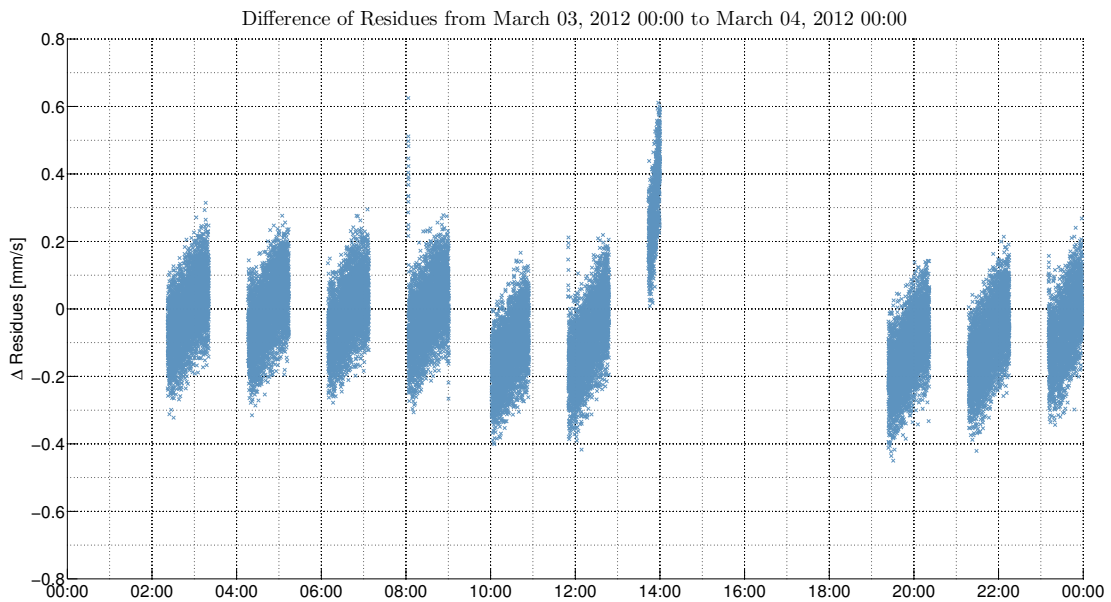


Figure 6.14.: Difference of computed observable with GEODYN solution
[Last iteration]

every observation time tag is with respect to the block integer second variable. The observation time also contains the fractional seconds. This time information is not interpretable at first glance, however, has the advantage that it is easily manageable and numerically stable. When converted to the [ET](#), the additional seconds are merely added to the observation time tag. In the course of the computation seconds are added and subtracted. Due to the format there is no need to control the correctness of the result in terms of format.

In the implemented routine the time tag is a common date format. This helps to interpret the results very easily. The downside is that every time a time is changed in the course of the calculation, its format has to be checked. Meaning that for example the second time tag has to be a value between zero and 60. And if a format is used incorrectly, it has to be revised. Due to this the computation time increased significantly.

Nevertheless in which format the time is, the accuracy of the computation falls and rises with the precision of the time tag. Therefore the number of decimal places and possible numerical issues are crucial. In the previous paragraphs two time formats were already mentioned. Additionally the time is needed in the Julian Date ([JD](#)) and the Modified Julian Date ([MJD](#)) for different functions. The [MATLAB](#) function *datenum* and the time and date utilities for [MATLAB](#) by [Acklam \(2010\)](#) are at first glance a great tool for this problem.

The function *datenum* converts a date to a numeric value as days since J2000.0. Additionally it allows to input incorrect date formats as described above. Unfortunately the precision is one millisecond, which is too low for the task. The function was therefore more or less completely substituted in the code. A similar problem emerges with the use of the time and date utilities. When converting a date to a [JD](#), decimal places are cut to accommodate the storage restrictions of [MATLAB](#). In this case the fractional seconds had to be replaced by the original date fractional seconds.

Chapter 7.

Conclusion

The motivation for this Master thesis was to use the **RS** technique in the case of **GRAIL**. **RS** is commonly used to determine the orbit and subsequently, the gravity field by observing the Doppler shift. This shift can be either measured in a 1-way, 2-way or 3-way mode. Since **RS** requires highly stable oscillators and is sensible to clock uncertainties the focus was solely laid on 2-way Doppler data.

To determine the orbit of **GRAIL** a dynamic orbit determination had to be performed. In the case of a dynamic orbit determination the orbit is predicted by modelling the forces acting upon the spacecraft and numerically integrating the trajectory. In a next step the computed observable is determined on the basis of the predicted orbit. At the end of the observation calculation process residuals were computed and used in a least-squares adjustment to fit the trajectory better to the observations. The main questions answered in this thesis are, what data is used, what happens to the data during its way of the processing and also how is the computed observable determined exactly.

In the case of **GRAIL** the **DSN** is tracking the spacecraft. The used data format is called **ODF** and is a time ordered list of the observations and also the different ramped frequencies for each station. For the use of the data in the software package **GEODYN**, which is used as a reference, the data had to be converted to the format **G2B**. In the conversion the data gets rearranged into data blocks of the same measurement type. Also observation specific information like the weather and the ramp information is included.

The actual range-rate determination starts with the light time solution and needs only the receiving time and counting interval as input parameters. The result of the solution is the reflection time at the spacecraft and the transmission time at the tracking station. Furthermore a range difference is calculated. Due to the fact, that in the case of interplanetary mission large distances are to be expected, the difference is expanded into a Taylor series. Afterwards the observation corrections (i.e. relativistic and tropospheric correction), frequency and counting interval are applied.

The actual value which is used in the following process of the orbit determination is the residual. This difference between the observed and the computed observation is also the

Chapter 7. Conclusion

value, which is compared to the reference residuals from [GEODYN](#). The result looks very promising. The difference is in the same magnitude as the measurement noise. The remaining trend in the data can be explained with a neglect of an center of integration correction of [GEODYN](#).

Further investigation for different time periods of the mission showed, that the presented results can be repeated at any given time for the case of [GRAIL](#). For other missions this process can be used as well, but has to adjusted accordingly. Since there seams not be a more precise tracking method for interplanetary missions, the [RS](#) method and therefore the Doppler shift have a bright future ahead. For future mission the usage of the band links may be rethought. Using a band link with a smaller wave length (e.g. Ka-band) would bring a better solution.

The presented solution is a solid result, but there are still improvements possible. Since the [GEODYN](#) solution was used as a reference some approximations and methods were adopted. For example the used tropospheric Hopfield model is outdated and could be replaced by a better model in an improved version. It also has to be noted that due to calculation limitations the coordinates had to be interpolated in between an one second sampling interval.

The shown process from the raw data to the residuals of the observations is just a small part of the orbit determination. The orbit determination as a whole is a very complex topic and the thesis at hand focusses only at a very small part of the whole procedure. Therefore a wide range of future research directions open up.

Bibliography

- Acklam, P. J. (2010). Time and Date Utilities. Source Code: <http://home.online.no/~pjacklam/matlab/software/util/timeutil/index.html>. Time and date calculation, Date representations, Time and date differences.
- Andert, T. P. (2010). *Masses of Small Bodies: Mass estimation of small solar system bodies using Radio Science data from close flybys*. PhD thesis, Universität zu Köln. <http://kups.ub.uni-koeln.de/id/eprint/3050>.
- Bae, T.-S. (2006). *Near Real-Time Precise Orbit Determination of Low Earth Orbit Satellites Using an Optimal GPS Triple-Differencing Technique*. PhD thesis, The Ohio State University. <https://etd.ohiolink.edu/>.
- Connally, M. (2006). TRK-2-24 DSN Tracking System Interfaces Weather Data Interface. Technical report, Jet Propulsion Laboratory, http://sbn.psi.edu/archive/dawn/grav/DWNVGRS_0/DOCUMENT/T2-24-L5.HTM. Deep Space Network (DSN) External Interface Specification, JPL D-16765.
- Dahiroc, P. (2013). Measurement Types. Technical report, <http://terra.sgt-inc.com/geodyn/documentation/volume5/CARDS/datastrucdop.html>. G2B Format Definition.
- Doody, D. (2001). *Basics of Space Flight*. Jet Propulsion Laboratory, <http://www2.jpl.nasa.gov/basics/index.php>. JPL D-20120, CL-03-0371, CL-11-1594 (PDF).
- DSN (2013). GRAIL ODF Metadata. http://pds-geosciences.wustl.edu/grail/grail-1-rss-2-edr-v1/grail_0201/odf/gralugf2011_253_1429smmv1.1b1. NASA/JPL Multi-Mission Navigation Radio Metric Data Conditioning Team.
- Fahnestock, E., Park, R., Yuan, D.-N., and Konopliv, A. (2012). Spacecraft thermal and optical modeling impacts on estimation of the GRAIL lunar gravity field. In *IAA/AAS Astrodynamics Specialist Conference 2012*, volume 1, pages 139–155. Guidance, Navigation, and Control and Co-located Conferences, American Institute of Aeronautics and Astronautics.
- Folkner, W. M. (1997). DSN Station Locations and Uncertainties. Technical report, Tracking System and Applications Section. TDA Progress Report 42-128.

Bibliography

- Hobbs, D. and Bohn, P. (2006). Precise Orbit Determination for Low Earth Orbit Satellites. *Annals of the Marie Curie Fellowship Association*, 4. <http://www.mariecurie.org/annals/volume4/mat2.pdf>.
- Hopfield, H. (1971). Tropospheric Effect on Electromagnetically Measured Range: Prediction from Surface Weather Data. *Radio Science*, 6(3):357–367. The Johns Hopkins University, Applied Physics Laboratory.
- Kahan, D. (2009). GRAIL Moon LGRS Derived Gravity Science Data Products V1.0, GRAIL-L-LGRS-5-RDR-V1.0. Technical report, Jet Propulsion Laboratory, http://pds.nasa.gov/ds-view/pds/viewHostProfile.jsp?INSTRUMENT_HOST_ID=GRAIL-A.
- Kahan, D. (2013). GRAIL Data Product Software Interface Specification. Technical report, Jet Propulsion Laboratory, http://pds-geosciences.wustl.edu/grail/grail-1-lgrs-2-edr-v1/grail_0001/document/dpsis.pdf. JPL D-76383.
- Konopliv, A. S., Park, R. S., Yuan, D.-N., Asmar, S. W., Watkins, M. M., Williams, J. G., Fahnstock, E., Kruizinga, G., Paik, M., Strelakov, D., Harvey, N., Smith, D. E., and Zuber, M. T. (2013). The JPL lunar gravity field to spherical harmonic degree 660 from the GRAIL Primary Mission. *Journal of Geophysical Research: Planets*, 118(7):1415–1434.
- Kwok, A. (2008). TRK-2-18 Tracking System Interfaces Orbit Data File Interface. Technical report, Jet Propulsion Laboratory, http://pds-geosciences.wustl.edu/grail/grail-1-rss-2-edr-v1/grail_0201/document/nav023_odf_2_18_rev3.htm. Deep Space Network (DSN) External Interface Specification, JPL D-16765.
- Liu, A. S. (1973). Range Measurements to Pioneer 10 Using the Digitally Controlled Oscillator. Technical report, Deep Space Network, http://ipnpr.jpl.nasa.gov/progress_report2/XIX/XIXI.PDF. The Deep Space Network Progress Report, TR 32-1526.
- McCarthy, J., Rowton, S., Moore, D., Pavlis, D., Lutcke, S., and Tsaoussi, L. (1993). *GEODYN II Systems Description*. Hughes STX Systems Corporation, 4400 Forbes Blvd., Lanham, MD 20706, 1 edition.
- Montenbruck, O. and Gill, E. (2001). *Satellite Orbits - Models, Methods, and Applications*. Springer-Verlag Berlin Heidelberg New York, 2nd edition.
- Moyer, T. D. (2000). Formulation for Observed and Computed Values of Deep Space Network Data Types for Navigation. In *JPL Deep-Space Communications and Navigation Series*, volume 1. John Wiley & Sons. 978-0-471-44535-7.

Bibliography

- NASA (2011). Gravity Recovery and Interior Laboratory (GRAIL) Launch. Press Kit. http://www.nasa.gov/pdf/582116main_GRAIL_launch_press_kit.pdf.
- Noreen, G. K. (1995). Deep Space Network Support of Small Missions. Technical report, Jet Propulsion Laboratory, California Institute of Technology, <http://www.upv.es/satelite/trabajos/pracGrupo15/Marte/DSN/PDF/Dsns.pdf>. Technical Session II: Mission Operations.
- Pavlis, D. and Wimert, J. (2013). Data Structure for Doppler Data. Technical report, <http://terra.sgt-inc.com/geodyn/documentation/volume5/CARDS/datastrucdop.html>.
- Petit, G. and Luzum, B. (2010). IERS Conventions (2010). Technical Report IERS Technical Note No. 36, International Earth Rotation and Reference Systems Service (IERS), <ftp://tai.bipm.org/iers/conv2010/tn36.pdf>.
- Ryne, M., Antreasian, P., Broschart, S., Criddle, K., Gustafson, E., Jefferson, D., Lau, E., Wen, H. Y., and You, T.-H. (2013). GRAIL Orbit Determination for the Science Phase and Extended Mission.
- Saastamoinen, J. (1973). Contributions to the Theory of Atmospheric Refraction. *Bulletin Géodésique (1946-1975)*, 107(1):13–34. National Research Council of Canada.
- Slobin, S. D. (2014). 301 Coverage and Geometry. Technical report, Deep Space Network, Jet Propulsion Laboratory, California Institute of Technology. DSN No.: 810-005,301, Rev.I, JPL D-19379.
- Thornton, C. L. and Border, J. S. (2000). *Radiometric Tracking Techniques for Deep-Space Navigation*. Jet Propulsion Laboratory, http://descanso.jpl.nasa.gov/monograph/series1/Descanso1_all.pdf. Deep Space Communications and Navigation Series.
- Turyshv, S. G. and Toth, V. T. (2006). The Pioneer Anomaly. *Canadian Journal of Physics*, 84(12):1063–1087.
- You, T.-H., Antreasian, P., Broschart, S., Criddle, K., Higa, E., Jefferson, D., Lau, E., Mohan, S., Ryne, M., and Keck, M. (2012). Gravity Recovery and Interior Laboratory Mission (GRAIL) Orbit Determination.
- Zuber, M. T., Smith, D. E., Lehman, D. H., Hoffman, T. L., Asmar, S. W., and Watkins, M. M. (2013a). Gravity Recovery and Interior Laboratory (GRAIL): Mapping the Lunar Interior from Crust to Core. *Space Science Reviews*, 178(1):3–24.
- Zuber, M. T., Smith, D. E., Watkins, M. M., Asmar, S. W., Konopliv, A. S., Lemoine, F. G., Melosh, H. J., Neumann, G. A., Phillips, R. J., Solomon, S. C., Wieczorek, M. A., Williams, J. G., Goossens, S. J., Kruizinga, G., Mazarico, E., Park, R. S.,

Bibliography

and Yuan, D.-N. (2013b). Gravity Field of the Moon from the Gravity Recovery and Interior Laboratory (GRAIL) Mission. *Science*, 339(6120):668–671.

Appendix A.

G2B Tracking Data Format

The format and content of the **G2B** files are specified on the **GEODYN** Homepage¹. The format is used to compute an orbit from radio metric data with the **GEODYN** program.

A **G2B** is a binary file and consists of radio metric data for one spacecraft and one or more stations. Within the file the information is stored in eight byte data blocks. One record consists of 10 eight byte words.

The data is grouped in logical blocks, consisting of different header and record types (Table A.1) distinguishable through the record indicator at the tenth place of the record. Each block contains data of a single type, between the same tracking stations and satellite, but recorded at different times (Pavlis and Wimert, 2013). Unlike the **ODF** format, all information concerning the observation of one logical block is stored together with the observations in the same block.

Record Type	Number	Indicator	Comment
Master Block Header Record	1	-9000000	Required
Block Header Record	1,2 or 3	-9000000+N*1000000 N=1,2 or 3	Required
Ramp Header Record	1	-5000000	Optional
Observation Record	Obs. No.	0	Required
Observation Corrections Record	Obs. No.	N*1000000 N=1,2 or 3	Optional
Ramp Data Record	Ramps/Block	6000000	Optional

Table A.1.: G2B layout (Pavlis and Wimert, 2013)

The header records of a block contain information about the observations in the logical block. The master header (Table A.2) with the indicator -9000000 contains the time

¹<http://terra.sgt-inc.com/geodyn>

Appendix A. G2B Tracking Data Format

information, measurement type and the observation record count in the block. Unlike in the ODF format, G2B associates different numbers with the measurement type. 1-way Doppler has assigned the number 42, 2-way Doppler the number 52 and 3-way Doppler the number 54 (Dahiroc, 2013). The block header (Table A.3) gives details over the reference frequency, station ID and satellite ID. Depending on the measurement type there are one or two header entries. In the case of 3-way Doppler data, another record is necessary for the second station ID. In the ramp header (Table A.4), the band link information is summarized. Additionally, the number of ramps in the block, the turn-around ratios and a bias are given. The bias is the transmitted reference frequency multiplied with the turn-around ratio.

Following the header records are the observation records (Table A.5) with the record indicator 0. Each observation has its own observation record entry with the observation, the counting interval as well as time information. After the observation information a observation correction record (Table A.6) follows. The meteorological data is formatted according to Table A.8 to fit the eight byte condition of the file format. The bytes are divided into humidity, pressure and temperature. The number of the observation correction records in each set are the same as the number of the observation records in the same block. The ramp information is only available if the data is ramped (Table A.7). The number of ramp records depends on the number of ramps covering the block of data. Included in the record are time stamps, the ramp rate as well as the start and end frequency of the ramp interval (Pavlis and Wimert, 2013).

Master Block Header Record	
1	Date and Integral Seconds of Data Pass Start Time in MJDS ²
2	Elapsed Time in Seconds from Pass Start to Data Block Start
3	Elapsed Time in Seconds from Data Block Start to Data Block End
4	Speed of Light Associated with Data in this Block
5	Measurement Type/Time System Indicator
6	Geodyn II Tracking Data Formatter version number used to create this file
7	Observation Record Count in Block
8	Number of Auxiliary Records Associated with Each Observation Record
9	Master Prepro Word
10	Record Type Indicator = -9000000

Table A.2.: G2B master block header record (Pavlis and Wimert, 2013)

Appendix A. G2B Tracking Data Format

Block Header Record	
1	0
2	0
3	Reference frequency (N=1 only)
4	0
5	0
6	Date and time this data file was formed
7	Station ID
8	Satellite ID
9	Prepro Word
10	Record Type Indicator = $-9000000+N*1000000$

Table A.3.: G2B block header record (Pavlis and Wimert, 2013)

Ramp Header Record	
1	Downlink Band ID (0=Ku, 1=S, 2=X, 3=Ka)
2	Uplink Band ID
3	Exciter Band ID
4	0
5	Number of Ramp Periods Covered (Two Ramps per Record Type 6000000)
6	Scale Factor 1 (Turn-Around Ratio) to Be Applied to the Receive Time Portion of the Ramp Interval (Usually 0)
7	Scale Factor 2 (Turn-Around Ratio) to Be Applied to the Transmit Time Portion of the Ramp Interval
8	Base Frequency of the Ramp Records (Add to Start Frequency of each Ramp)
9	Reference Frequency scaled by Turn-Around Ratio (Table 3.2)
10	Record Type Indicator = -5000000

Table A.4.: G2B ramp header record (Pavlis and Wimert, 2013)

Appendix A. G2B Tracking Data Format

Observation Record	
1	Observation
2	Doppler Counting Interval
3	Sum of Observation Corrections
4	0
5	Sum of Time Corrections
6	Elapsed Time from Block Start to Time of Observation in Seconds
7	Observation Sigma
8	0
9	0
10	Record Type Indicator = 0

Table A.5.: G2B observation record (Pavlis and Wimert, 2013)

Observation Correction Record	
1	Meteorological Data for Station
2	Spacecraft Center of Gravity Correction
3	Dry Tropospheric Refraction for Station
4	Wet Tropospheric Refraction for Station
5	Antenna Axis Displacement Correction for Station
6	Ionospheric Refraction
7	Ionospheric Refraction
8	Relativity Correction for Station
9	Transponder Delay Doppler Correction for Satellite
10	Record Type Indicator = N000000

Table A.6.: G2B observation correction record (Pavlis and Wimert, 2013)

Ramp Record	
1	Elapsed UTC Seconds since J2000 at Start of Ramp Interval
2	Elapsed UTC Seconds since J2000 at End of Ramp Interval
3	Transmit Frequency at Start of Ramp Interval (Hz)
4	Transmit Frequency Rate of Change (Hz/s)
5	Elapsed UTC Seconds since J2000 at Start of Ramp Interval
6	Elapsed UTC Seconds since J2000 at End of Ramp Interval
7	Transmit Frequency at Start of Ramp Interval (Hz)
8	Transmit Frequency Rate of Change (Hz/s)
9	0
10	Record Type Indicator = 6000000

Table A.7.: G2B ramp record (Pavlis and Wimert, 2013)

Appendix A. G2B Tracking Data Format

Bit	Item	Format and Unit
0-13	Humidity	0.01 %
14-31	Pressure	0.01 Millibars
32-47	Temperature	0.01 Degree Kelvin

Table A.8.: G2B weather data (Pavlis and Wimert, 2013)

Appendix B.

Tracking Data Format Conversion

To determine the orbit with **GEODYN**, the measured data from the **DSN** has to be converted into a readable format for **GEODYN**. For this conversion a routine, previously used for **MESSENGER**, was adapted to fit the case of **GRAIL**. As an input parameter the **ODF** as well as the **WEA** files are used. Additional information about the light time between spacecraft and tracking station (**LIGHTTT**), the satellite id (**SATID**) and the leap seconds (**LEAPSECOND**) are incorporated (Fig. B.1). The leap seconds are provided in **GEODYN**'s Earth orientation file called **gdntable.data**.

Throughout the conversion process the data is not changed, only rearranged. In a sample **ODF** (Listing B.1) and **G2B** (Listing B.2) file, the differences are demonstrated. The mentioned data quantities in the following paragraphs are important for the further calculation process. The quantities in the text, as well as their respective values in the listing, are framed in the same color.

The most sensible data is the time. While the **ODF** time tag is at the middle of the counting interval, **GEODYN** expects the time tag at the end of the count interval. In the **ODF** listing the time information is given as **UTC** seconds since the reference time. The **reference time** can be found in the file header and has the format **YYYYMMDDMMHHSS**. The **observation time tag** is the first item in the list, while the **ramp start** and **ramp end time** is in the first and last column of the ramp information block. Opposed to this the **G2B** observation time tag is given as **MJDS UTC** seconds. The information is split into three parts: the seconds till the data pass start time, the elapsed seconds from pass start to data block start and the elapsed time from block start to the time of the observation. The addition of the three time informations give the observation time tag. The ramp start and ramp end time in the **G2B** are in **UTC** seconds since J2000.0.

The observations in the **ODF** are time-ordered, regardless of the measurement type. This can be seen in column eight of the observation block, containing the **measurement type** values. The **2-way Doppler data** is afterwards blocked and can be found in the **G2B** file. The measurement type in the **G2B** file can be found in the header, since observations of the same type are blocked together. Here it can be seen that the 2-way Doppler data of

Appendix B. Tracking Data Format Conversion

the ODF results in a 3-way Doppler data in the G2B file. This is a normal modification due to the conversion routine, since GEODYN treats 2-way and 3-way Doppler data the same. In this way, the transmitting station can be treated differently than the receiving station (even at the same site) to account for the difference in epochs. Also the counting interval changes its format from hundredth of seconds to seconds.

The ramp start frequency of the ODF is split into the ramp base frequency in the header and the residual transmitting frequency in the ramp information block. The change rate stays the same.

Newly added is the weather information in the third G2B data block in the first column. This block exists twice, due to the fact that there are two (different) stations involved in the 3-way Doppler measurement. Temperature, pressure and relative humidity can be decoded with the help of the information in Table A.8.

Additionally the band links, satellite and station IDs are available in the files. While each observation record in the ODF contains the information, in the G2B format it is compressed in the header. Furthermore the turn-around ratio and a bias can be found in the ramp header of the G2B.

Appendix B. Tracking Data Format Conversion

B.1. LIGHTT File

The LIGHTT File is an [ASCII](#) file and it is necessary to assign the correct ramp record to each observation. Each line of the light time file has an epoch in [MJD](#) and the approximated number of light seconds to the satellite at that epoch. The light time can be extracted from the LTM1A File of the [PDS](#). This information is particularly important in the case of interplanetary spacecraft. Regarding [GRAIL](#) the information can be neglected.

Listing [B.3](#) shows the first lines of the LIGHTT file. Every ten seconds a new value for the light time is available. As evident in the listing below, the quantities are quite similar. That is why in the case of [GRAIL](#) the file is not necessary for the computation, but for the correct execution of the conversion routine.

Listing B.3: LIGHTT file

55987.416780	1.342433
55987.416896	1.342440
55987.417012	1.342447
55987.417127	1.342453
55987.417243	1.342458
55987.417359	1.342464
55987.417475	1.342469
55987.417590	1.342474
55987.417706	1.342478

B.2. SATID File

The SATID File is an [ASCII](#) file and allows to stamp the record with the correct satellite ID. [G2B](#), and therefore [GEODYN](#), uses a seven digit satellite ID. The SATID file contains only the seven digit satellite ID, which is then used in the new [G2B](#) file. The satellite ID of [GRAIL-A](#) is 1104601.

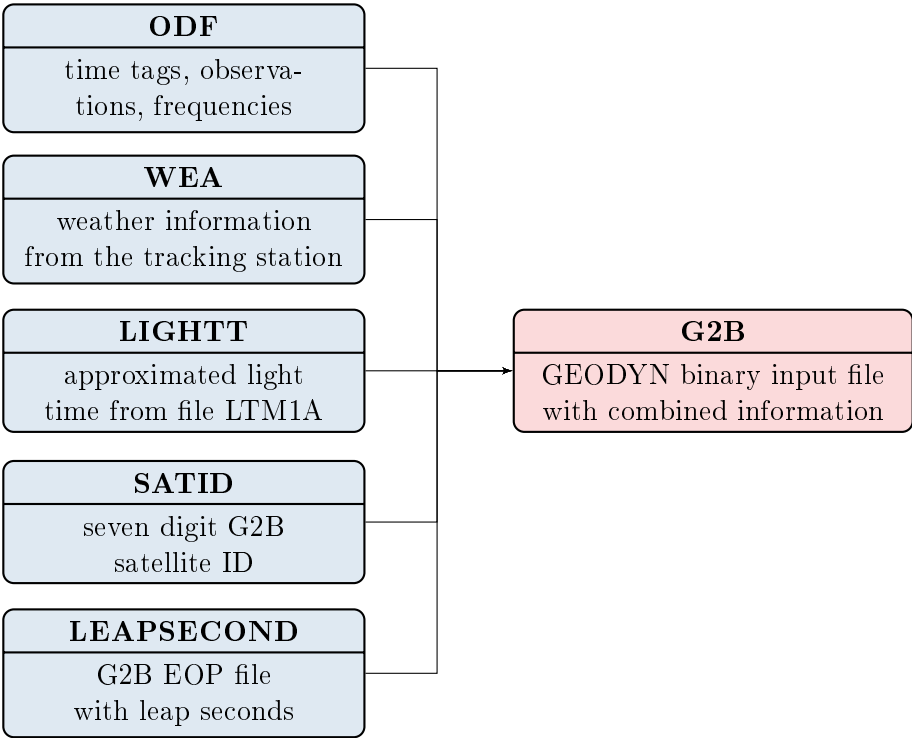


Figure B.1.: Conversion process

Appendix C.

GEODYN II

In the present work the implemented observation computation with Doppler data was compared to the results of the software package [GEODYN II](#). It has been written by the [NASA GSFC](#) in Fortran IV and has been operational since 1985.

[GEODYN II](#) is used extensively for applications in the field of satellite geodesy including determination of orbits, tracking instrumentation calibration, satellite predictions, and geodetic parameter estimation. It has the capability to estimate a set of orbital elements, station positions, measurement biases, and a set of force parameters (e.g. gravity field spherical harmonic coefficients) such that the orbital tracking data best fits the entire set of estimation parameters.

C.1. Input

[GEODYN](#) is a powerful and flexible tool for a range of different problems in the field of satellite geodesy. This flexibility causes extreme variation in the input. The two major inputs are the observation data and the [GEODYN](#) input cards. These cards control the detailed specification of the problem to be solved. Setting options include:

- Cartesian orbital elements,
- satellite drag coefficients,
- satellite emissivity,
- station positions,
- geopotential coefficients,
- Earth tidal parameters,
- satellite cross-sectional area,
- satellite mass,

- integration times for the orbit,
- epoch time of elements and
- solar and geomagnetic flux.

Also the integration and data editing can be controlled. The printed output can be specifically modified and consists usually of the measurements and residuals, as well as residual and solution summaries.

Additionally the planetary ephemeris, a gravity field and flux data are needed. [GEODYN](#) uses the [JPL](#) export ephemeris for nutation, positions, and velocities of the Moon, Sun, and planets ([McCarthy et al., 1993](#)).

C.2. Modelling

The orbit determination reacts very sensible to the initial state vector. Hence the coordinates for the vector were taken from a [JPL GRAIL](#) orbit product. The satellite parameter mass is detailed in the Lunar Gravity and Ranging System ([LGRS](#)) Experimental Data Record ([EDR](#)) Level 0 data product called MAS00, which can be found in the [PDS](#) ([Kahan, 2013](#)). The satellite cross sectional area can be found in [Fahnestock et al. \(2012\)](#). The epoch time was chosen to last two days. Due to instability issues less than one day of determination is not recommended. More time was rejected considering the overall computation time. Also the time interval was selected such, that during this time was no orbit manoeuvre.

The most influential gravitational force is the central body or center of integration, which in the case of [GRAIL](#) is the Moon. Therefore a gravity field up to degree and order 270 was chosen. The used gravity model GL0660B from [Konopliv et al. \(2013\)](#) was determined from data of the primary mission of [GRAIL](#). Additionally the figure of the Earth and especially the oblateness of the Earth have a considerable influence.

From the non-gravitational forces the solar radiation pressure is the most influential force. Since a simple implementation was chosen, there is a lot of room for improvement. According to [Ryne et al. \(2013\)](#) in order to model the solar radiation pressure force, the physical structure of the spacecraft has to be decomposed into a seven-component model by [Fahnestock et al. \(2012\)](#). In this model every surface of the spacecraft is represented by a plate with coefficients corresponding to the material and its characteristics.

The most prominent factor in the present modelling is the general acceleration (also known as empirical accelerations). The orbit prediction reacts strong to different model variations. The chosen option was to estimate a constant along-track quantity.

C.3. Processing

Since [GEODYN](#) has grown over 30 years, the program structure is very complex. The following functions are an important part of the computation of the observable. Additionally the flow chart in [Fig. C.1](#) displays the links and connections of the different subroutines and functions.

The main function of the software package is the function `EXEC2E`. There the script `OBSGEN` for the observation determination is invoked. The function `OBSGEN` is the main subroutine for the observation determination of all measurement types. In the case of Doppler data, with the measurement type value in between 36 and 96, the subroutine `METRIC` is called.

The light time solution as well as the determination of the observation corrections are calculated in the function `ROBS`. Due to the [GRAIL](#) constellation of tracking stations and spacecraft the function `MTSTST` is responsible for the determination of the light time solution.

The orbit integration and interpolation is driven by the function `ORBIT`. The numerical integration is accomplished by the Cowell's method in the function `COWELL`. The positions of the celestial bodies, as well as the time corrections between the [TDT](#) and [TDB](#), are determined in the function `COORDT`.

Function `LITPRX` is only used in the case that the satellite is orbiting, and therefore integrated around a different body than the tracking station is located on. Its task is to calculate initial values for the reflection time t_2 and the transmission time t_1 . If the initial guess of the light time is close to the final result, the iteration in the functions `LITEUP` and `LITEDN` converges already after the first or second pass. Hence the time needed for the calculation gets shortened significantly.

Function `LITEUP` computes the light time between the tracking station at receiving time t_3 and the spacecraft at reflection time t_2 . It is assumed that the receiving time t_3 is known. For the reflection time t_2 the result of the function `LITPRX` is used as an initial value and is determined in an iterative process. Also the general relativistic light time and the relativistic correction for the [TDB](#) is computed.

Function `LITEDN` computes the light time between satellite at time t_2 and the tracking station at transmission time t_1 . It is assumed that the reflection time t_2 is known. For the transmission time t_1 the result of the function `LITPRX` is used as an initial value and is determined in an iterative process. Also the general relativistic light time and the relativistic correction for the [TDB](#) is computed.

The observation corrections are computed and summarized in function `ROBSUM`. Dependent on the measurement type the adequate model for the meteorological correction

Appendix C. GEODYN II

is selected. In the case of [GRAIL](#) the Hopfield model is selected (Function HOPFLD). Also the relativistic correction is determined.

Function INTPRM computes the 1-way or 2-way range difference for an interplanetary satellite using Chebyshev polynomial differencing. As input parameter the determined times of the function LITEUP and LITEDN are used. Afterwards the observation corrections calculated in ROBSUM are subtracted.

In the functions RAMPRR and RMPGRL the frequency is applied to the observable. The large constant part of the current ramp interval is determined in the function RAMPRR, while in the function RMPGRL the smaller part, based on the ramps, gets calculated. As a final step the computed observable is differenced by the counting interval in function AVGRR. The residues are computed in the function PROCES. As of iteration two a station dependent measurement bias from the least squares adjustment is removed from the residuals in function BIASES.

Appendix C. GEODYN II

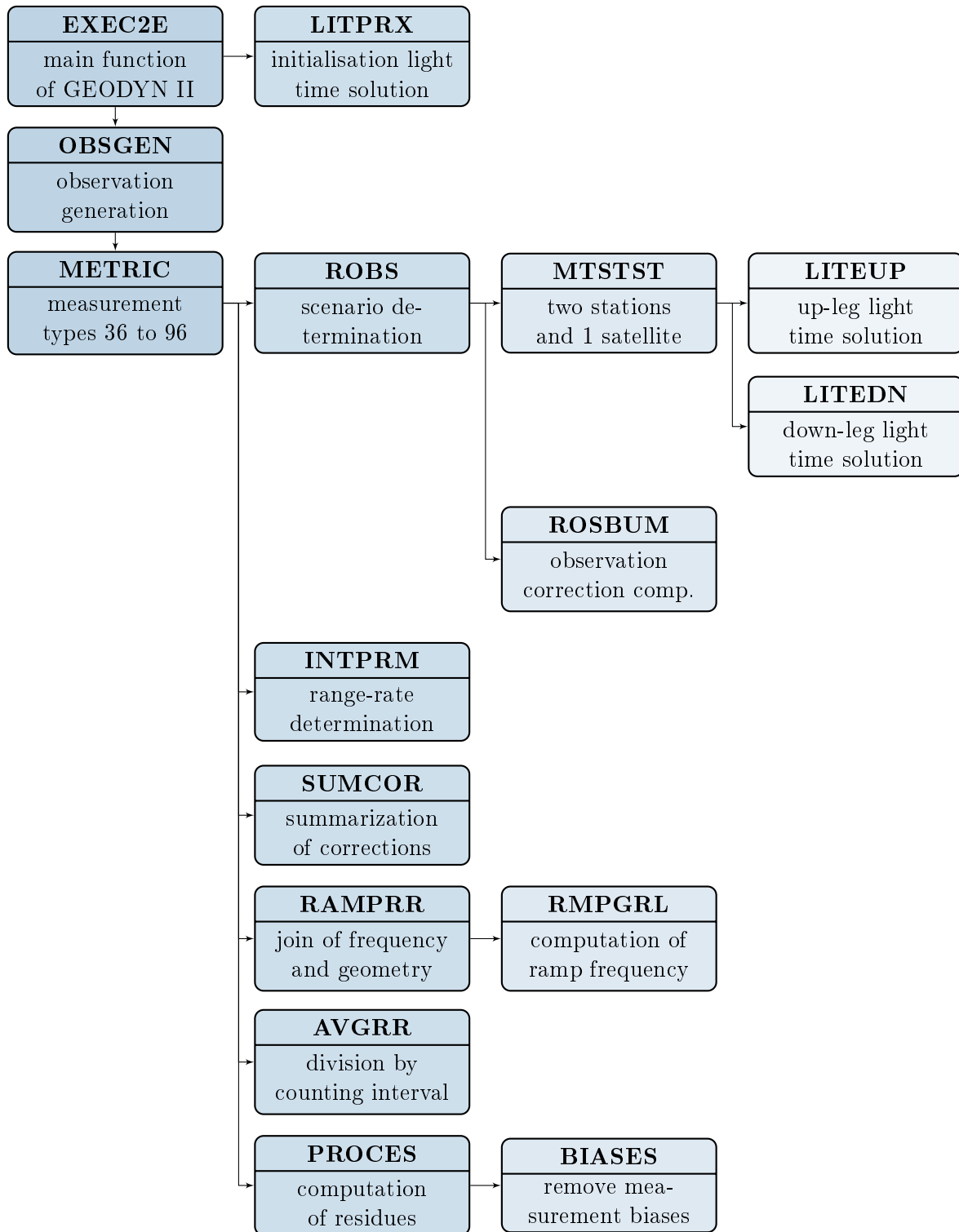


Figure C.1.: Observation generation in GEODYN II